NASA-CR-205688

Micro and Macro Segregation in Alloys Solidifying With Equiaxed Morphology

NCC8-57

Final Report

submitted to

George C. Marshall Space Flight Center

by

Doru M. Stefanescu, PI, The University of Alabama, Tuscaloosa

Peter. A Curreri, CoPI, MSFC, Huntsville

Jose Leon-Torres, Gr. Res. Asst., The University of Alabama, Tuscaloosa

Subhayu Sen, MSFC, Huntsville

ABSTRACT

To understand macrosegregation formation in Al-Cu alloys, experiments were run under terrestrial gravity (1g) and under low gravity during parabolic flights (10^{-2} g). Alloys of two different compositions (2% and 5% Cu) were solidified at two different cooling rates. Systematic microscopic and SEM observations produced microstructural and segregation maps for all samples. These maps may be used as benchmark experiments for validation of microstructure evolution and segregation models.

As expected, the macrosegregation maps are very complex. When segregation was measured along the central axis of the sample, the highest macrosegregation for samples solidified at 1g was obtained for the lowest cooling rate. This behavior is attributed to the longer time available for natural convection and shrinkage flow to affect solute redistribution. In samples solidified under low-g, the highest macro-segregation was obtained at the highest cooling rate. In general, Low-gravity solidification resulted in less segregation.

To explain the experimental findings, an analytical (Flemings-Nereo) and a numerical model were used. For the numerical model, the continuum formulation was employed to describe the macroscopic transports of mass, energy, and momentum, associated with the microscopic transport phenomena, for a two-phase system. The model proposed considers that liquid flow is driven by thermal and solutal buoyancy, and by solidification shrinkage.

The Flemings-Nereo model explains well macrosegregation in the initial stages of low-gravity segregation. The numerical model can describe the complex macrosegregation pattern and the differences between low- and high-gravity solidification.

1. INTRODUC. ON

During alloy solidification, a region where the liquid and solid phases coexist, the mushy zone, travels across the sample. Understanding of phenomena occurring in the mushy zone is of paramount importance to the production of castings with required properties. Casting defects such as macro- and micro-segregation, and porosity have their origin in the mushy zone. In particular, macrosegregation is formed because of the existence of non uniform composition at the macroscopic level resulting from solute redistribution affected by fluid flow, and transport of solid fragments in and out of the mushy zone. Macrosegregation produce important variations of the physical and mechanical properties in castings, degrading their possible use. The above reasons are the motivation to study the mechanism of macrosegregation formation and the possibilities to reduce macrosegregation.

Few reliable data exist to document macrosegregation. Some data were generated by Flemings and Nereo [1,2,3] and Kato and Cahoon [4]. In the same papers, Flemings and Nereo proposed a macrosegregation model, assuming that the interdendritic flow is driven only by solidification contraction, and ignoring solid phase movement. The "local redistribution equation". was derived.

Diao and Tsai [5] developed a model using the "continuum formulation" based on the classical mixing theory valid in the entire casting, including the solid and liquid phases and the mushy zone, developed by Bennon and Incropera [6]. Complete diffusion in liquid and solid and no solid movement were assumed. This model was improved by Chang and Stefanescu [7] by assuming complete diffusion in liquid and no diffusion in solid, and by allowing the equiaxed grains to move with the liquid until dendrite coherency was reached.

When solidification occurs under low-gravity conditions, the interdendritic flow is driven only by shrinkage. Thus, low-gravity research simplifies the problem and allows easier understanding of macrosegregation formation. To the best of our knowledge, only Favier *et al.* [8] have reported data in low gravity conditions using aluminum-copper alloys. Unfortunately, they do not present the whole composition field, in particular for the initial transient solidification.

Maples and Poirier [9] considered the effects of 0-g in their model using equations for convection coupled with the local redistribution equation. They concluded that no macrosegregation is obtained in the casting. Krane and Incropera [10] discussed buoyancy and shrinkage effects in macrosegregation using the continuum formulation, separating natural convection from shrinkage, and analyzing the influence of both driving forces. Their analysis of shrinkage can be applied to low gravity. Assuming that the only driving force is shrinkage, they predicted macrosegregation close to the chill. Additionally, it was predicted that macrosegregation will increase with the cooling rate. This last point is in contradiction with the Diao-Tsai model which predicts lower macrosegregation with higher cooling rate.

The main purpose his study was to generate data for mac gregation in the presence and in the absence of natural convection. This last condition was obtained using low gravity during solidification to eliminate gravity driven convection.

2. EXPERIMENTAL PROCEDURE

Aluminum-copper alloys with 2% and 5% copper were melted in a resistance furnace. The liquid metal was treated with pure argon for 20 minutes, and poured in a cylindrical mold, having a cavity of 10 mm in diameter and 25 mm in length. These samples were instrumented with K-type thermocouples. Two types of experiments were run, ground based and in a low-gravity (Low-g) environment during parabolic flights on board a NASA DC-9 aircraft. The experimental hardware used was the Isothermal Casting Furnace.

During the experiments the temperature and the gravity level were continuously recorded.

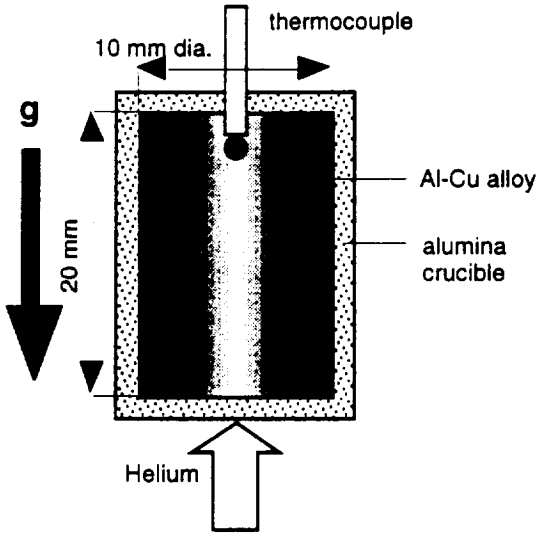

Fig. 1 Drawing of crucible - sample assembly.

All samples were homogenized at 680 °C for 40 min. At this temperature, the alloy is completely liquid. Following the homogenization period, the samples were quenched by blowing helium gas through the bottom of the heating unit (Fig. 1). By controlling the needle valve between the pressurized helium gas tank and the heating unit, two different cooling rates were obtained, 9 °C/sec and 15 °C/sec.

For the parabolic flight experiments, each sample was quenched during the third low gravity maneuver. The cooling curve and accelerometer data indicated that the samples were completely solidified during the low gravity period. Four samples were produced for each gravity condition.

The samples run and the levels of the monitored variables are presented in Table 1 . Characterization included the followings:

- Metallographic examination for microstructure mapping.

- Micropı ; analysis to evaluate the macrosegrega. ı. A bean-diameter of 200 μm was used. This was sufficient to check macrosegregation because the dendrite arm spacing was smaller than 20 μm.

Table 1 Experimental samples and variables

Sample no.	Copper, %	g-level	Cooling rate, K/s
1 / 5HgHCR	5	ground	15
2 / 5LgHCR	5	low	15
3 / 5HgLCR	5	ground	9
4 / 5LgLCR	5	low	9
5 / 2HgHCR	2	ground	15
6 / 2LgHCR	2	low	15
7 / 2HgLCR	2	ground	9
8 / 2LgLCR	2	low	9

3. EXPERIMENTAL RESULTS

3.1 Microstructure

The typical microstructure of all samples showed columnar grains. All samples were examined for primary and secondary dendrite arm spacing. The SDAS varied within rather narrow limits for all samples, between 10 and 25 μm, as shown for selected samples in Fig. 2. This is not surprising, since SDAS is mostly a function of the local solidification time. However, the primary spacing (PDAS) showed a clearer variation (Fig. 3). Indeed, the sample solidified under High-g had a maximum PDAs of 185 μm, as compared with a maximum of 155 μm for the sample solidified in Low-g. This is probably a consequence of solid grain transport during solidification. For Low-g solidified samples, increasing the cooling rate from 9 to 15 °C/s did not seem to make a significant difference.

(see next pages)

Fig. 2 SDAS distribution across selected experimental castings.

(see next pages)

Fig. 3 PDAS (in μm) distribution across two experimental castings.

3.2 Macrosegregation

The experimental results are presented as plots of the copper content along the central axis of the samples (Fig) and as macrosegregation maps. The significance of these results is rather complex and their interpretation is not straight forward. In general, macrosegregation is higher for the samples solidified in High-g. This can be observed on Fig. 4 and Fig. 5, when

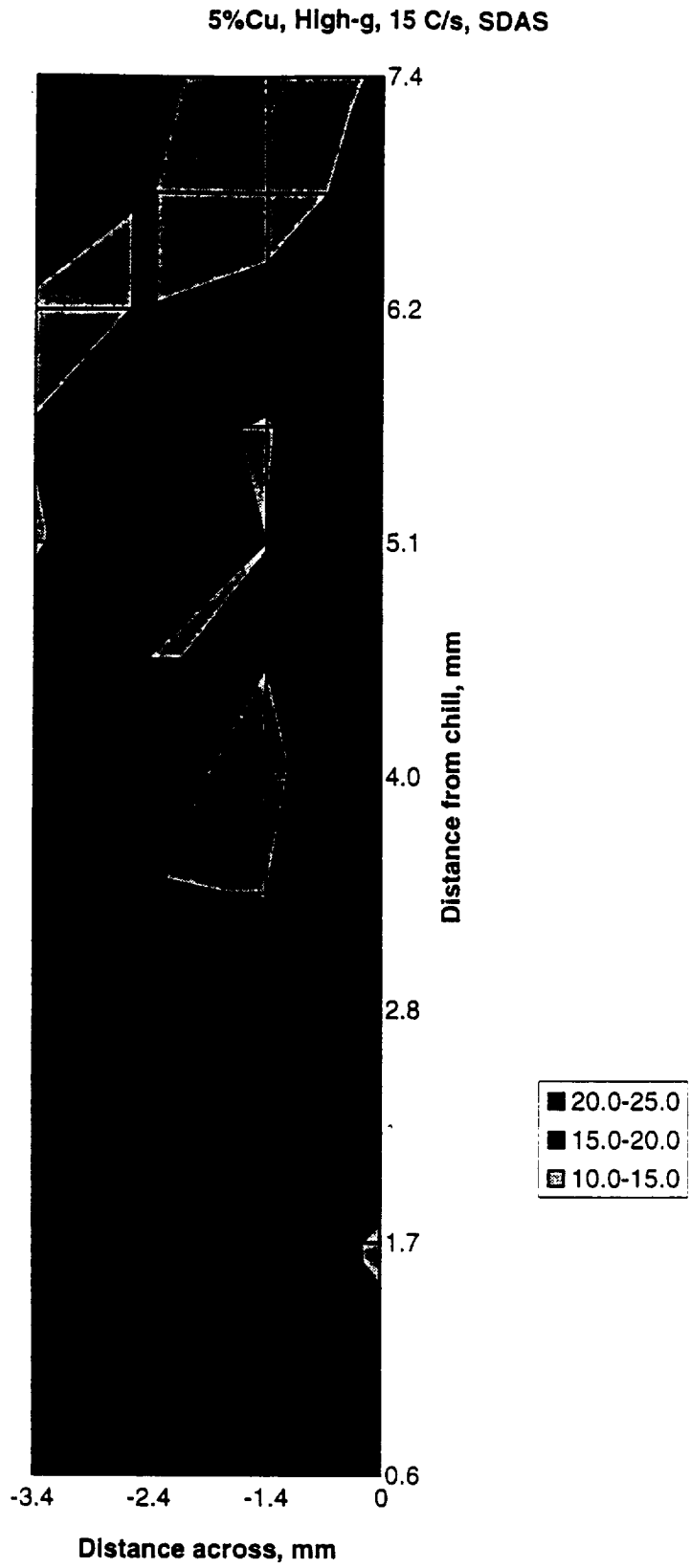
5%Cu, High-g, 15 C/s, SDAS
7.4
6.2
5.1
4.0
2.8
1.7
0.6
Distance from chill, mm
20.0-25.0
15.0-20.0
10.0-15.0
-3.4
-2.4
-1.4
0
Distance across, mm

Fig. 2 SDAS

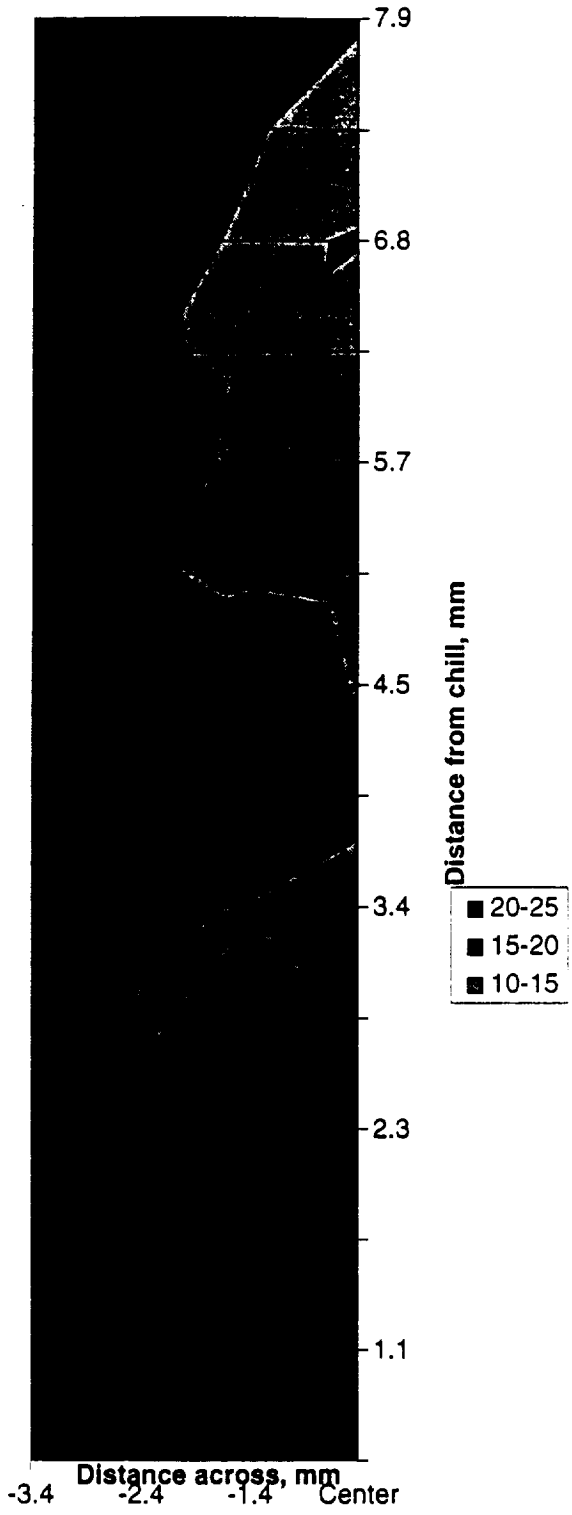
5% Cu, Low-g, 9 C/s, SDAS
7.9
6.8
5.7
4.5
3.4
2.3
1.1
Distance from chill, mm
20-25
15-20
10-15
Distance across, mm
-3.4
-2.4
-1.4
Center

Fig. 2 SDAS

2%Cu, High-g, 9 C/s, PDAS

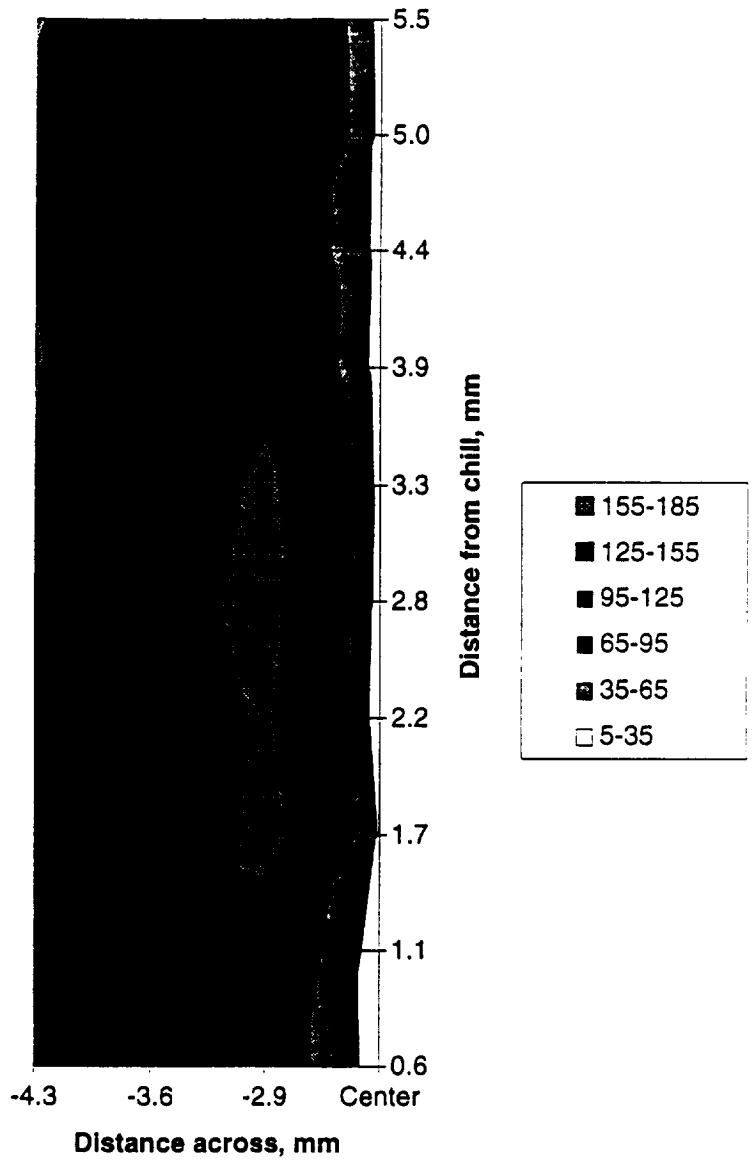

Fig. 3 PDAS

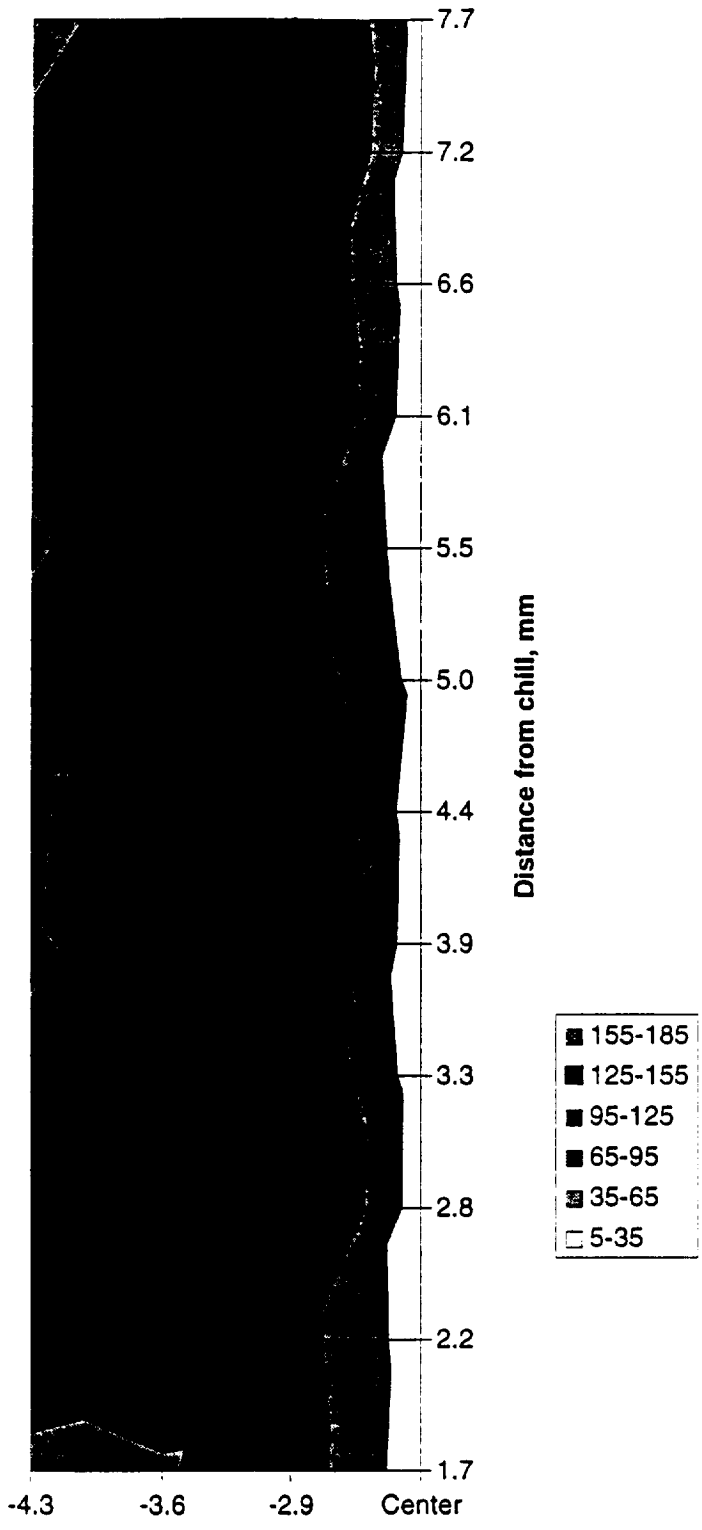
2%Cu, Low-g, 9 C/s, PDAS
7.7
7.2
6.6
6.1
5.5
5.0
4.4
3.9
3.3
2.8
2.2
1.7
Distance from chill, mm
155-185
125-155
95-125
65-95
35-65
5-35
-4.3
-3.6
-2.9
Center
Distance across, mm

Fig. 3 PDAS

comparing the di: :nce between the maximum positive .d negative segregation. For example, for samples having 2% Cu and being cooled at 9 °C/s this difference is of 0.8% for the High-g sample as compared with only 0.5% for the Low-g sample. Also, segregation is higher for the slower cooled samples.

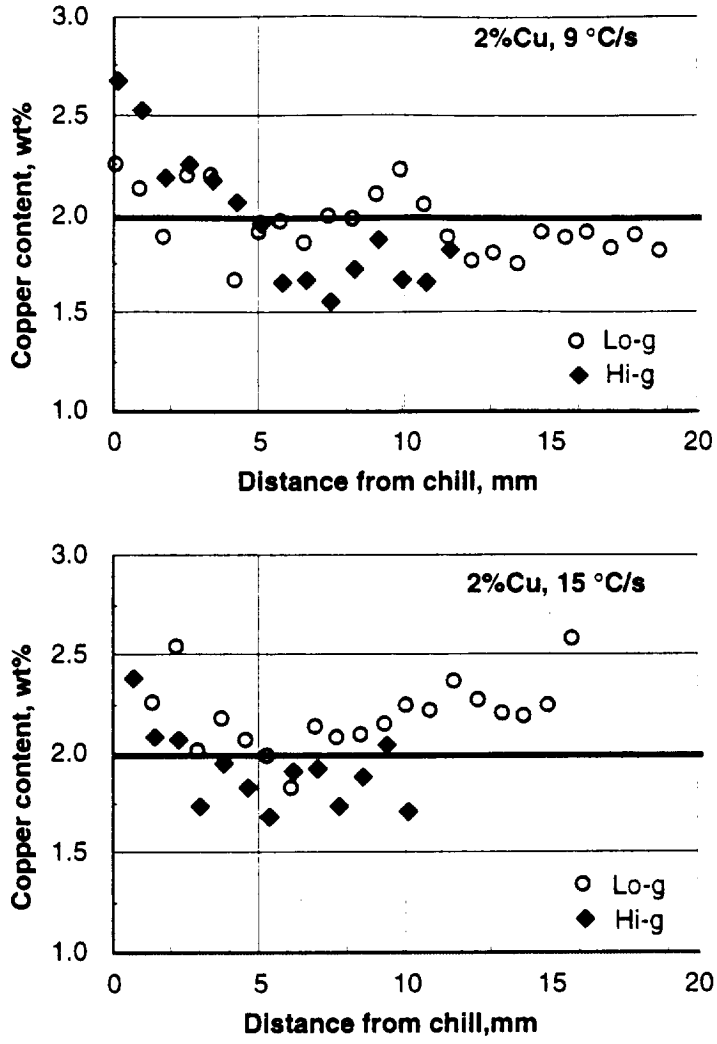

Fig. 4 Experimental data for copper variation across the longitudinal axis of the sample as a function of gravity level and cooling rate for 2% Cu samples.

As seen when comparing Fig. 4 and Fig. 5, segregation increased considerably when the Cu content was raised from 2 to 5%.

The maps of copper segregation are, not unexpectedly, very complex. They are presented in Fig. 6 and Fig. 7. The region showed in white was not measured. It was occupied by the thermocouple or by shrinkage voids. For the samples solidified under High-g a higher cooling rate seem to decrease macrosegregation (compare Hi-g, 9 °C/s with Hi-g, 15 °C/s in Fig. 7). Indeed the region having a copper content of 1.8 - 2.2%, which is close to the initial average composition, is larger in the sample solidified at 15 °C/s. Less segregation appears in the slow cooled Low-g sample.

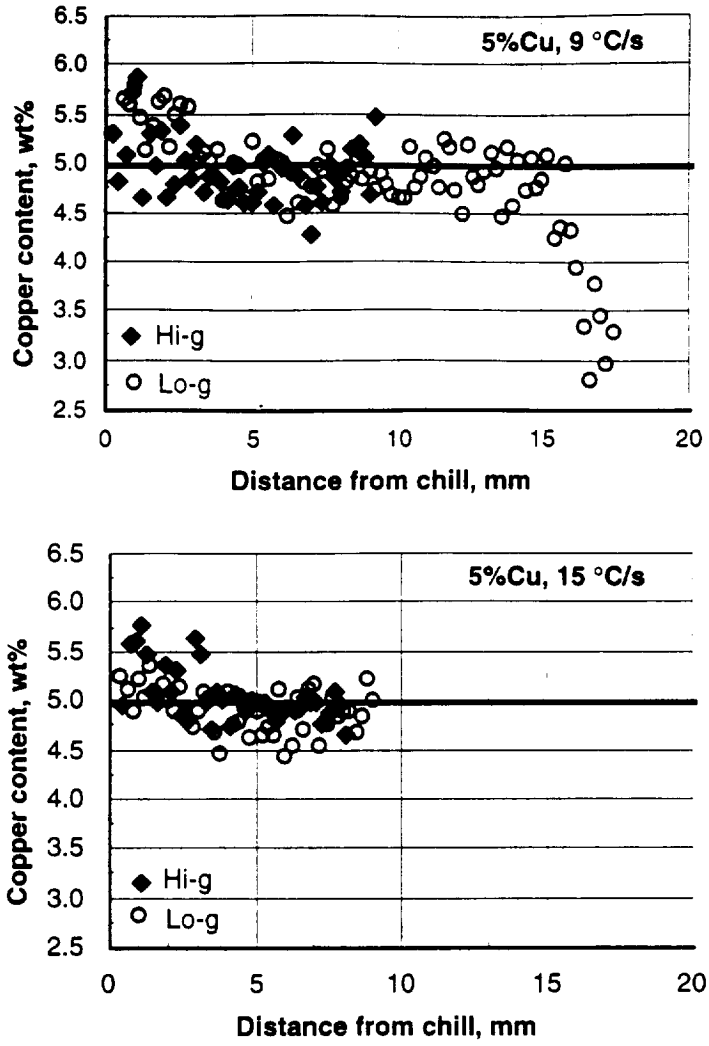

Fig. 5 Experimental data for copper variation across the longitudinal axis of the sample as a function of gravity level and cooling rate for 5% Cu samples.

(see next pages)

Fig. 6 Experimental map of copper segregation for Al-5% Cu samples solidified under various gravity conditions and cooling rates.

(see next pages)

Fig. 7 Experimental map of copper segregation for Al-2% Cu samples solidified under various gravity conditions and cooling rates.

4. MODELING TECHNIQUES

Three different modeling approaches were used in this study, as follows:

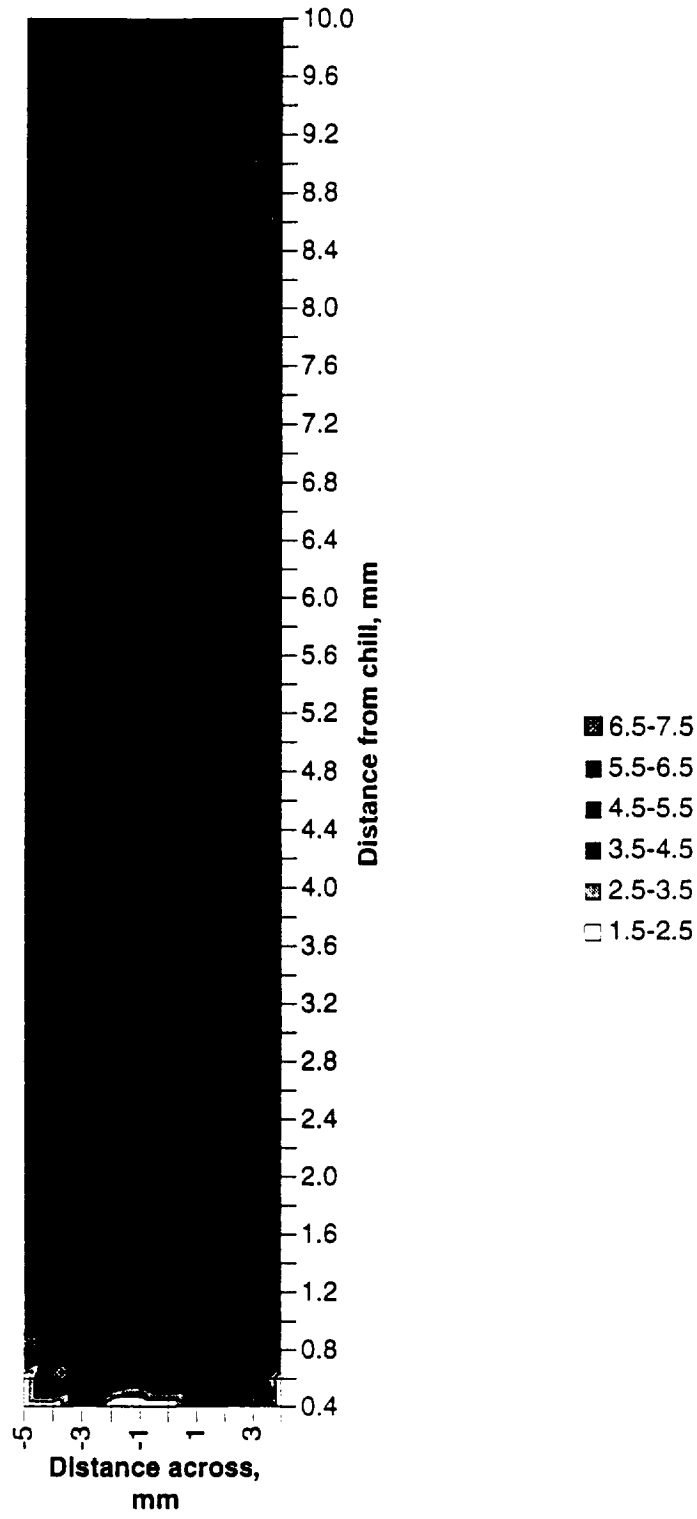

Fig. 6 Macrosegregation map

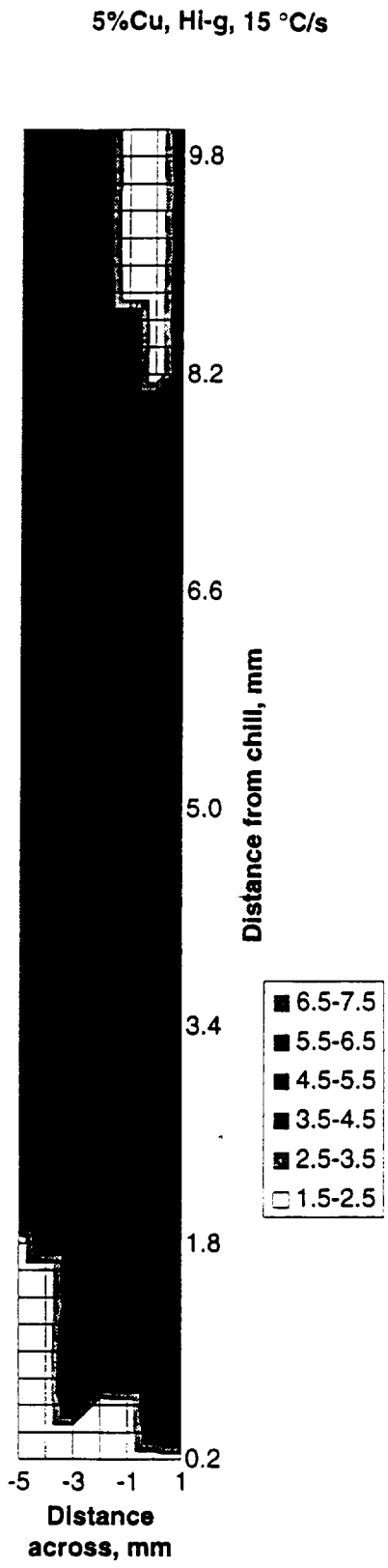

Fig. 6 Macrosegregation map

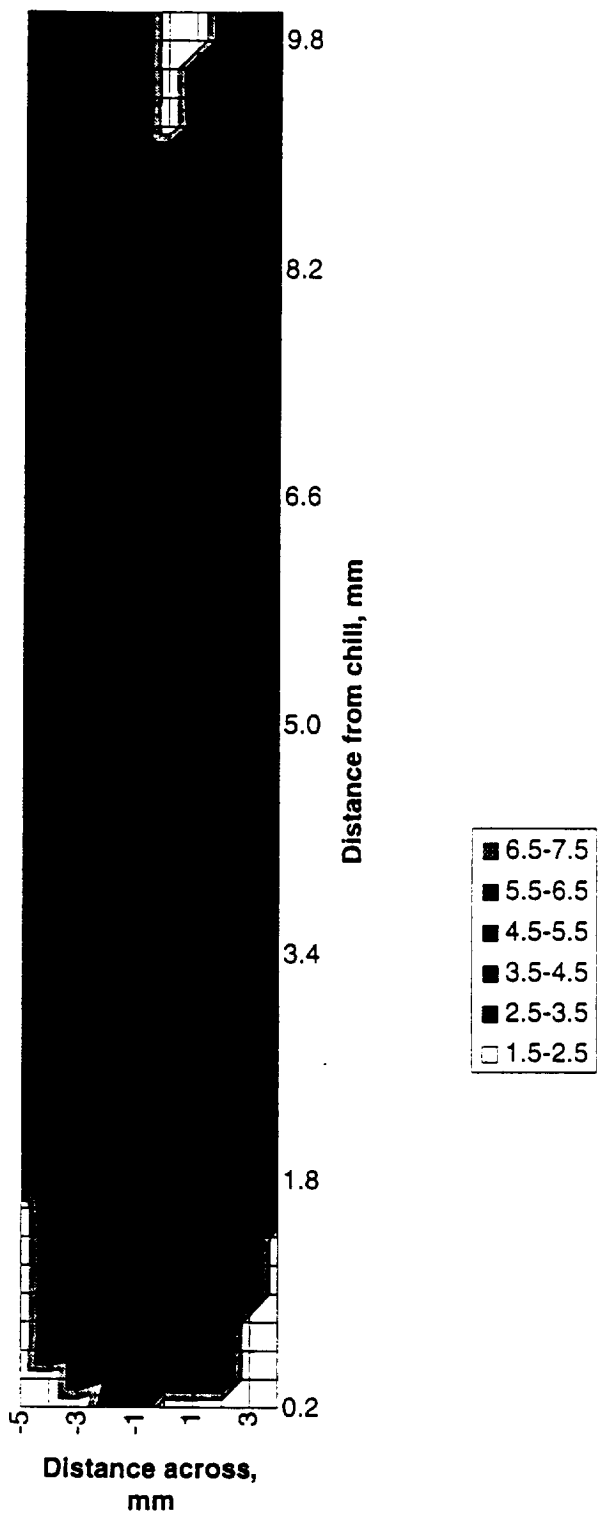

Fig. 6 Macrosegregation map

5%Cu, Hi-g, 15 °C/s

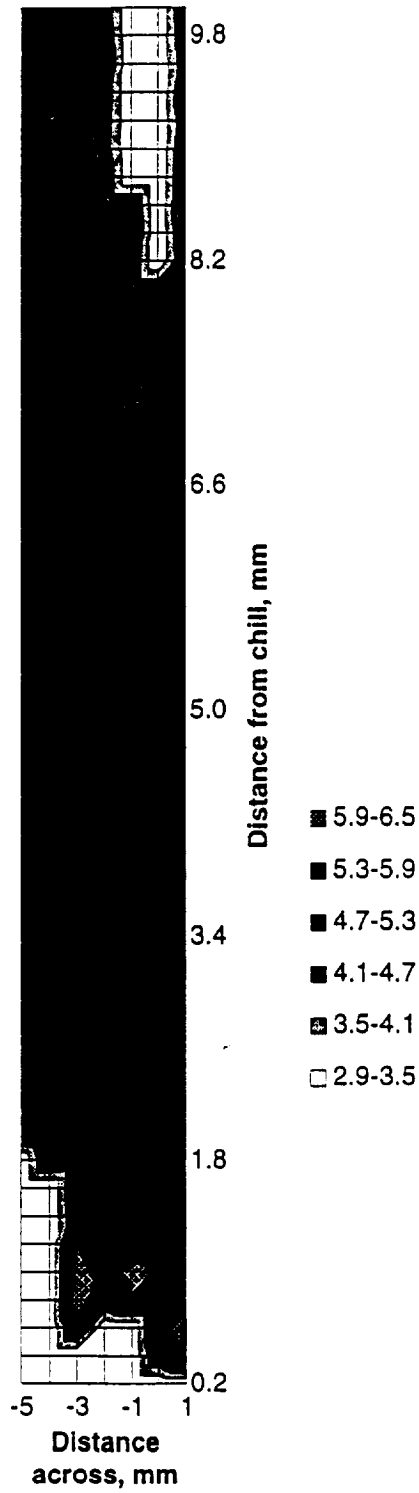

Fig. 6 Macrosegregation map

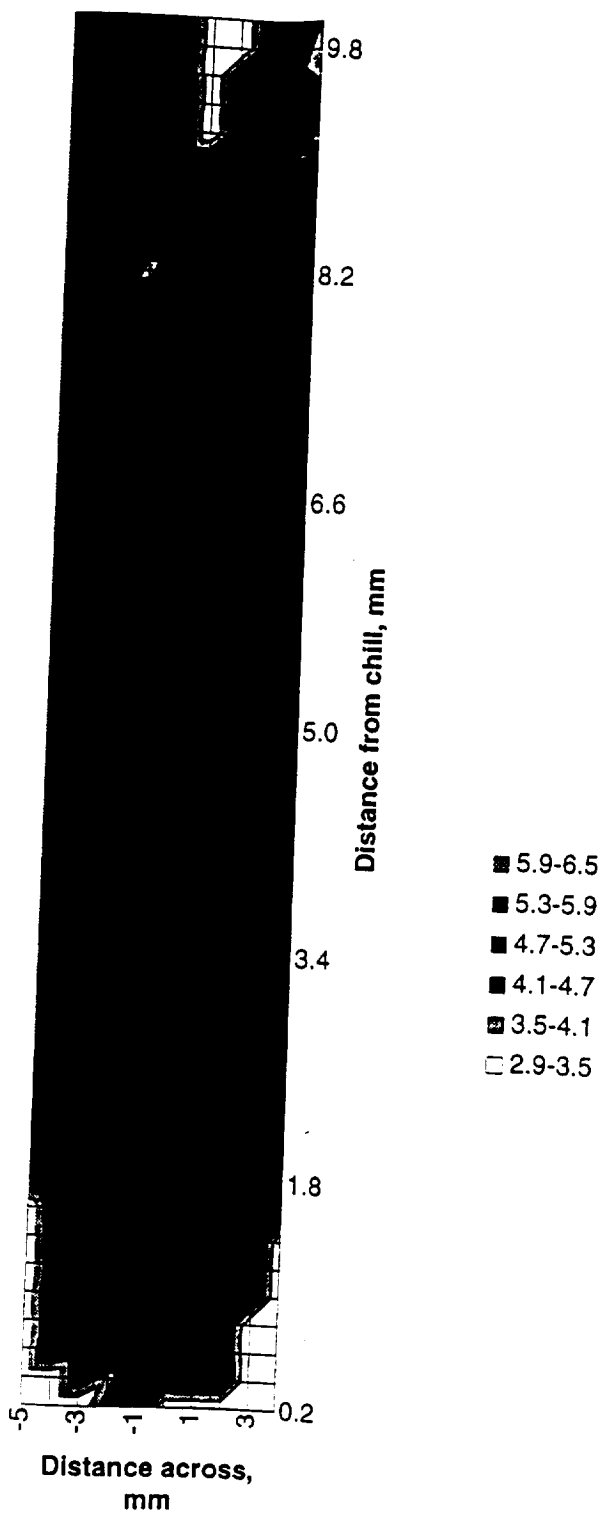

Fig. 6 Macrosegregation map

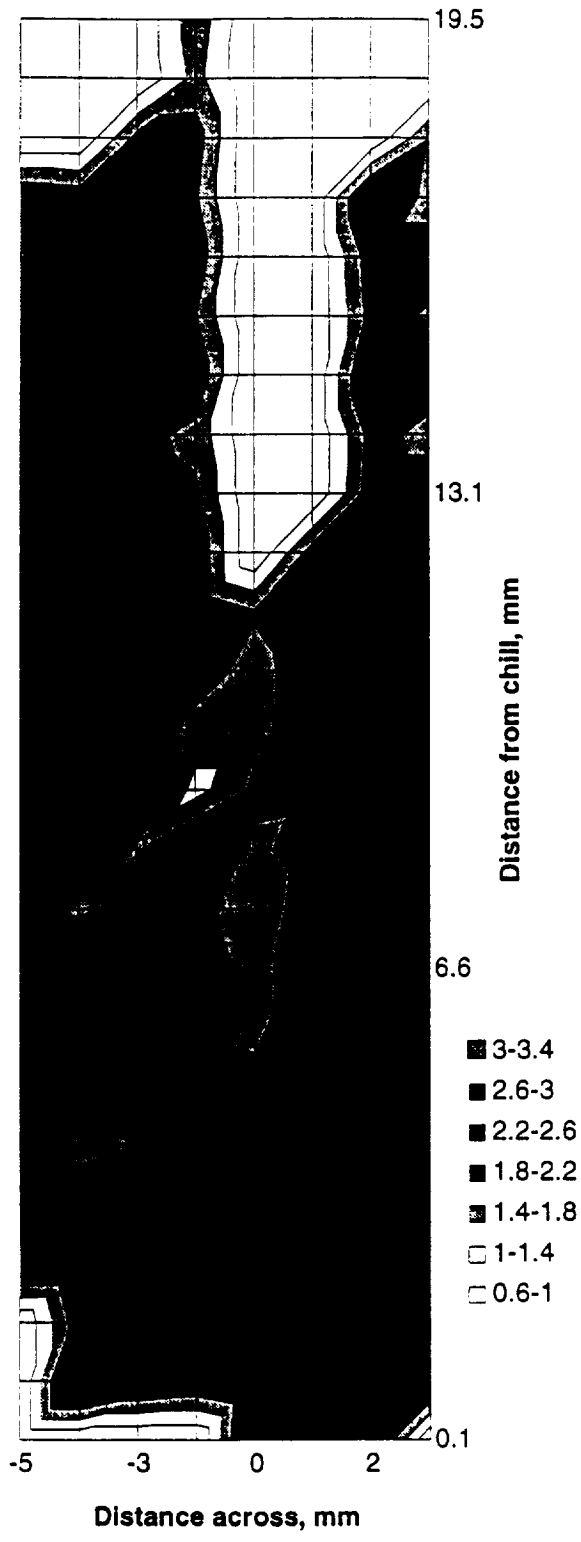

Fig. 7 Macrosegregation map

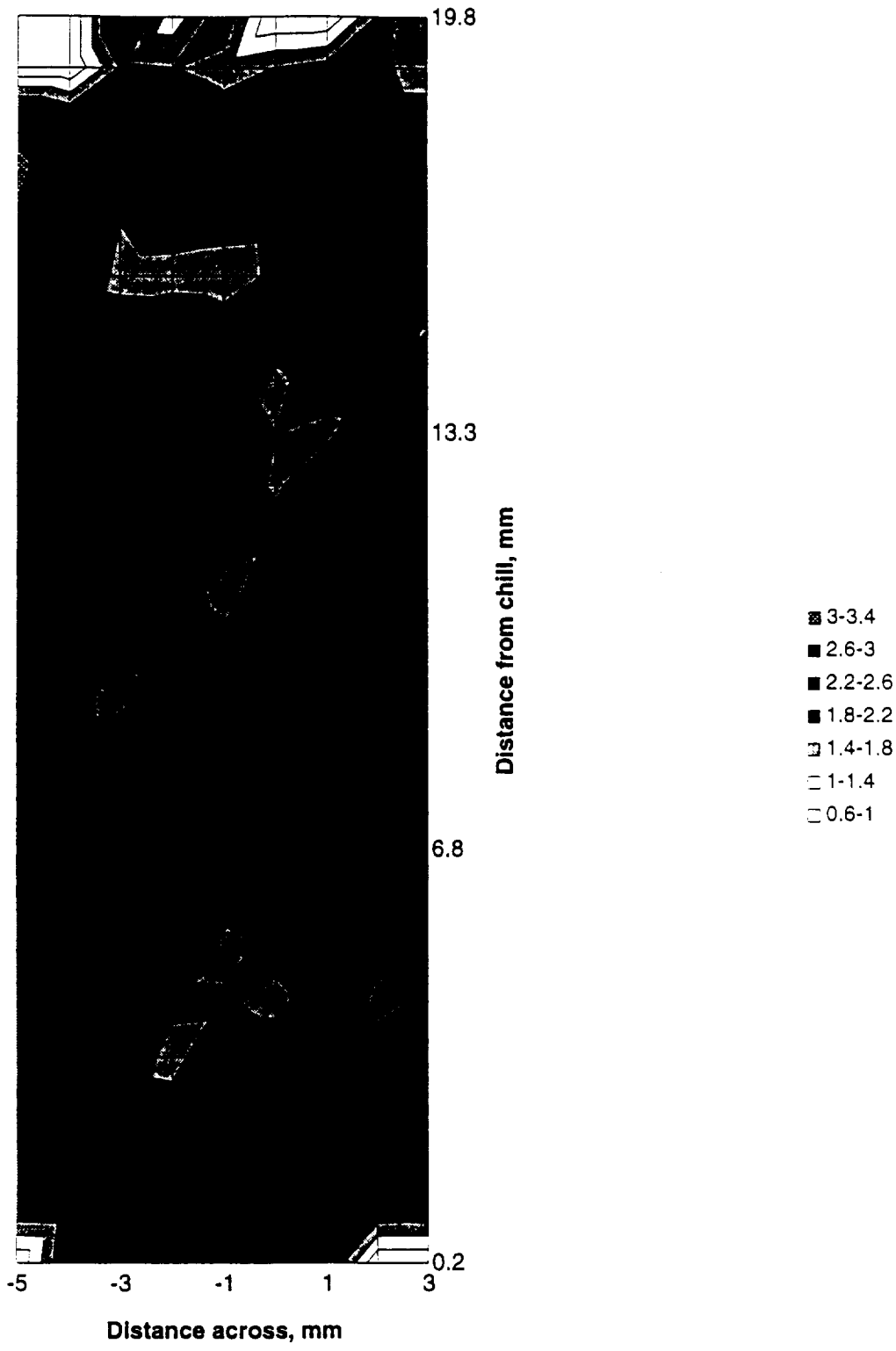

Fig. 7 Macrosegregation map

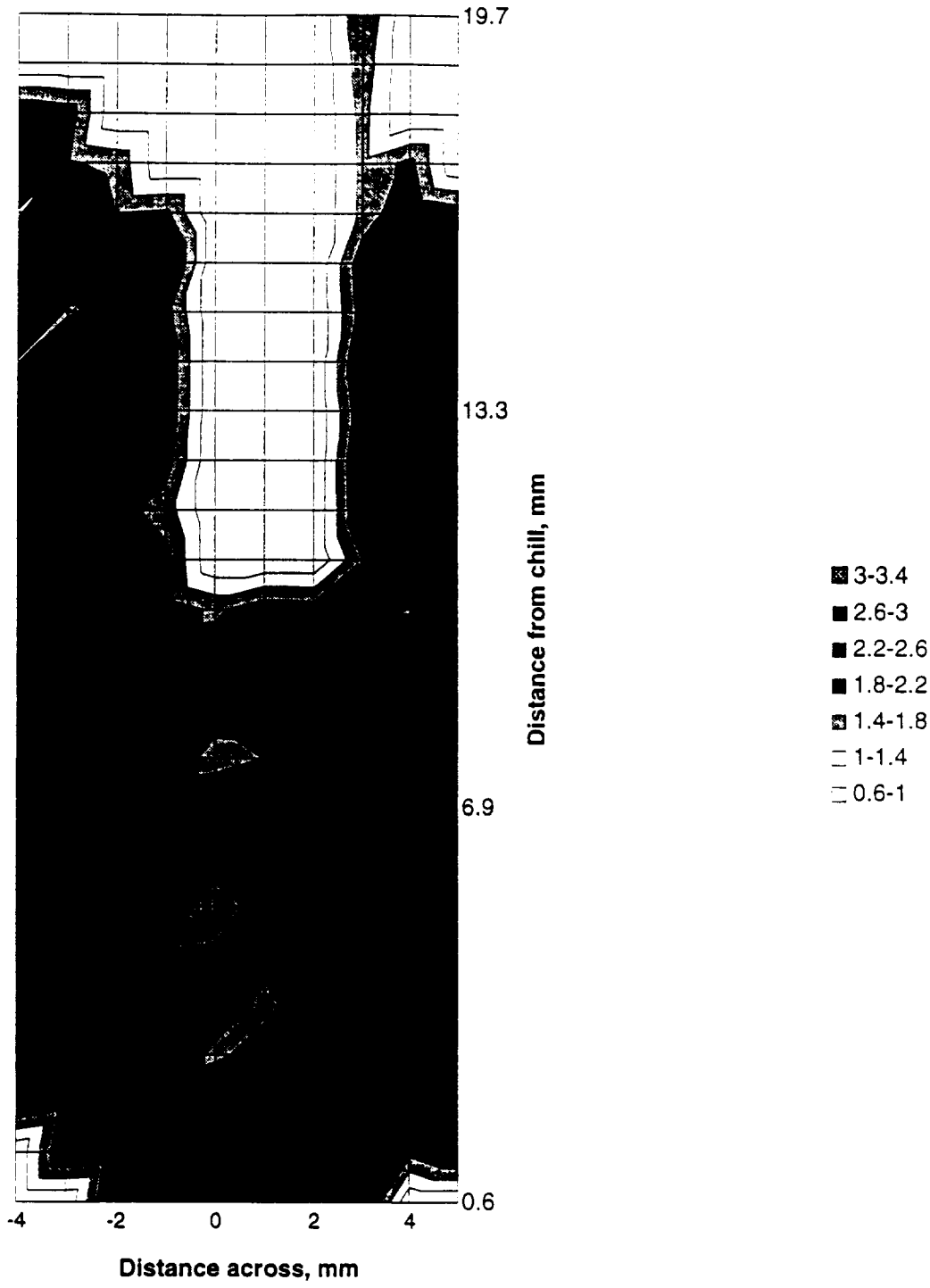

Fig. 7 Macrosegregation map

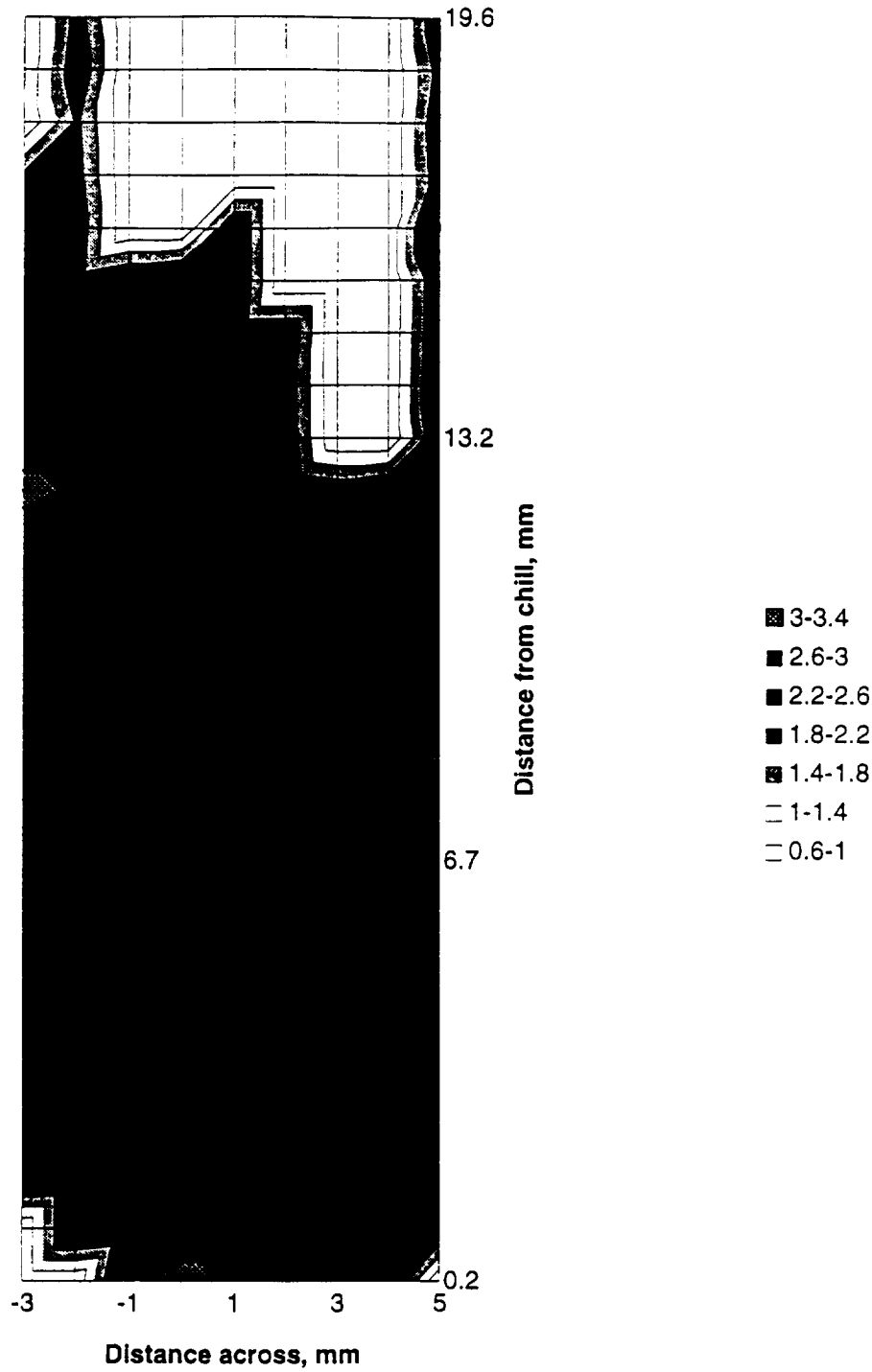

Fig. 7 Macrosegregation map

- an analytical model for macrosegregation adapted after the analytical model proposed by Flemings and Nereo [1];
- an analytical model for microsegregation; this model is a further development of a previous model [11] based on the "closed system" assumption (no net mass transport in or out the domain during solidification);
- a numerical model for macrosegregation, which is an extension of the model proposed by Chang and Stefanescu [7].

4.1 The analytical macrosegregation model

The assumptions made in the Flemings-Nereo model are as follows: negligible convection in the bulk liquid; macrosegregation results from the interdendritic flow of solute-rich liquid to feed thermal and solidification contraction; no solid material enters or leaves the volume element during solidification; solute enters or leaves the element only by liquid flow to feed shrinkage; mass in or out of the element by diffusion is neglected; liquid composition and temperature are uniform within the element; no diffusion in solid; constant densities; the fraction of liquid is assumed to vary linearly with temperature within the mushy zone; no pores formation. With these assumptions the local solute redistribution equation was derived:

Eq. 1
$$\frac{\partial g_L}{\partial C_L} = -\left(\frac{1-\beta}{1-k}\right)\left(1+\frac{V\cdot\nabla T}{dT/dt}\right)\frac{g_L}{C_L}$$

where g_L is the fraction of liquid, C_L is the liquid concentration, β is the shrinkage ratio, k is the partition coefficient, V is the fluid velocity, T is the temperature, and t is the time. This equation was integrated, and macrosegregation was calculated with:

Eq. 2
$$\overline{C}_S = \frac{\rho_S \int_0^{1-g_E} C_S \partial g_S + \rho_{SE}\, g_E\, C_E}{\rho_S(1-g_E)+\rho_{SE}\, g_E\, C_E}$$

where ρ is the density, C is the composition, g is the fraction of phase, and the symbols E and S stand for eutectic and solid, respectively.

To use the above equations for calculation of macrosegregation it is necessary to provide data for the term $\frac{V\cdot\nabla T}{dT/dt}$. By obtaining the movement of the liquidus, solidus and eutectic isotherms with a 2-D energy transport model, this term was calculated using the approach described in ref. [1]. The curves were plotted on the graphs showing the axial variation of Cu (see for example Fig. 4 and Fig. 5).

4.2 The analytical microsegregation model

A comprehensive analytical micro-segregation model, that considers diffusion in both solid and liquid phases, and relaxes the closed system assumption, was developed. It solves the

'Fickian' diffusion h time-independent diffusion coefficie and non zero-flux boundary conditions for systems solidifying with equiaxed morphology. The model that has general validity takes into account solute transport in the solid and liquid phases and includes overall solute balance. Since the model does not require a prescribed movement of the interface, it can be used for microscopic modeling of solidification. The model allows calculation of liquid and solid compositions, during and after solidification, for spherical geometry (equiaxed grains). It also includes coarsening and coalescence that take place during solidification. It can be used for concentration profile calculations for systems that solidify with equiaxed grains, whether eutectic (*e.g.*, lamellar graphite-austenite, Al-Si) or dendritic (*e.g.*, Al-alloys, Fe-low C alloys, superalloys).

A paper has been published describing the model and its application [12]. A copy of this paper is attached to this report.

4.3 The numerical model

The assumptions made in Chang-Stefanescu model are as follows: shrinkage - induced and natural convection in the bulk liquid; each finite volume can be occupied by liquid and solid phases simultaneously (no pore formation); complete diffusion in liquid and no solid diffusion. The solidification process is divided into two stages: in the first stage, the solid and liquid phases are moving together and the relative velocity is zero; in the second stage, no solid movement occurs after dendritic coherency (relative viscosity increases when the fraction of solid increases). The following macroscopic transport equations are used:

Continuity

Eq. 3 $$\frac{\partial \rho}{\partial t}+\nabla.(\rho V)=0$$

Conservation of momentum

x-momentum

Eq. 4 $$\frac{\partial}{\partial t}(\rho u)+\nabla.(\rho V u)=\nabla.\left(\mu^{*}\nabla\frac{\rho}{\rho_L}u\right)-\frac{\partial p}{\partial x}-\frac{\mu^{*}}{K}(u-u_S)-\nabla.(\rho f_L f_S V_r u_r)$$
$$-\frac{C\rho^{2}}{K^{1/2}\rho_L}|u-u_S|(u-u_S)$$

y-momentum

Eq. 5 $$\frac{\partial}{\partial t}(\rho v)+\nabla.(\rho V v)=\nabla.\left(\mu^{*}\nabla\frac{\rho}{\rho_L}v\right)-\frac{\partial p}{\partial x}-\frac{\mu^{*}}{K}(v-v_S)-\nabla.(\rho f_L f_S V_r v_r)$$
$$+\rho_0 g[\beta_T(T-T_0)+\beta_C(C_L-C_{L,0})]-\frac{C\rho^{2}}{K^{1/2}\rho_L}|v-v_S|(v-v_S)$$

Conservation of Energy

Eq. 6 $\frac{\partial}{\partial t}(\rho c_p T) + \nabla.(\rho c_p V T) = \nabla.(k \nabla T) - \nabla.(L \rho g_s (V - V_s)) - \frac{\partial}{\partial t}(L \rho g_s) - \nabla.(L \rho_L g_L V)$

Conservation of Mass

Eq. 7 $\frac{\partial}{\partial t}(\rho C) + \nabla.(\rho C V) = \nabla.(\rho D \nabla C) + \nabla.(\rho D \nabla(C_L - C)) - \nabla.(\rho f_s (V - V_s)(C_L - C_s))$

where $V (= u\hat{i} + v\hat{j})$ is velocity, $V_r (= V_L - V_S)$ is relative velocity, p is pressure, μ^* is the relative viscosity, f is the fraction of phase, β_T and β_C are the thermal and solutal expansion coefficients respectively, C_p is the specific heat, k is the thermal conductivity, L is the latent heat of fusion, the subscripts L, S, and 0 stand for liquid, solid, and liquidus respectively. Also, $C = 0.13 \cdot f_L^{3/2}$. Eq. 2 was used to calculated the local average composition in the sample solidified.

This equations were solved using the SIMPLER algorithm [13]. The boundary conditions were in principle, as described in ref. [7].

5. DISCUSSION

It was generally found in this research that high (normal) - gravity solidification results in higher macrosegregation than low - gravity solidification. This was illustrated, for example, in Fig. 4 for axial measurements. This is not surprising since in High-g liquid convection results from both natural convection and shrinkage flow, while only shrinkage flow is driving segregation in Low-g. Thus, the composition should be more uniform in samples solidified under Low-g.

However the picture is not that simple. The complexity of segregation maps makes interpretation difficult. Changing the range of composition plotted may alter the apparent segregation pattern.

To evaluate the Flemings-Nereo model some calculated curves were plotted against the experimental data in Fig. 8. The Flemings-Nereo model seems to work reasonably well at the beginning of solidification in Low-g. The compliance with the experimental data is less good for High-g solidification. Since this model is based on the assumption that flow is driven only by solidification shrinkage this is not surprising. The model predictions increasingly diverge from the experimental results with increased distance from chill. It is indeed impossible for an analytical model to describe the complexities of macrosegregation toward the end of solidification, where a rapid increase in negative segregation occurs, in particular at high copper contents (curve for 5% Cu on Fig. 8).

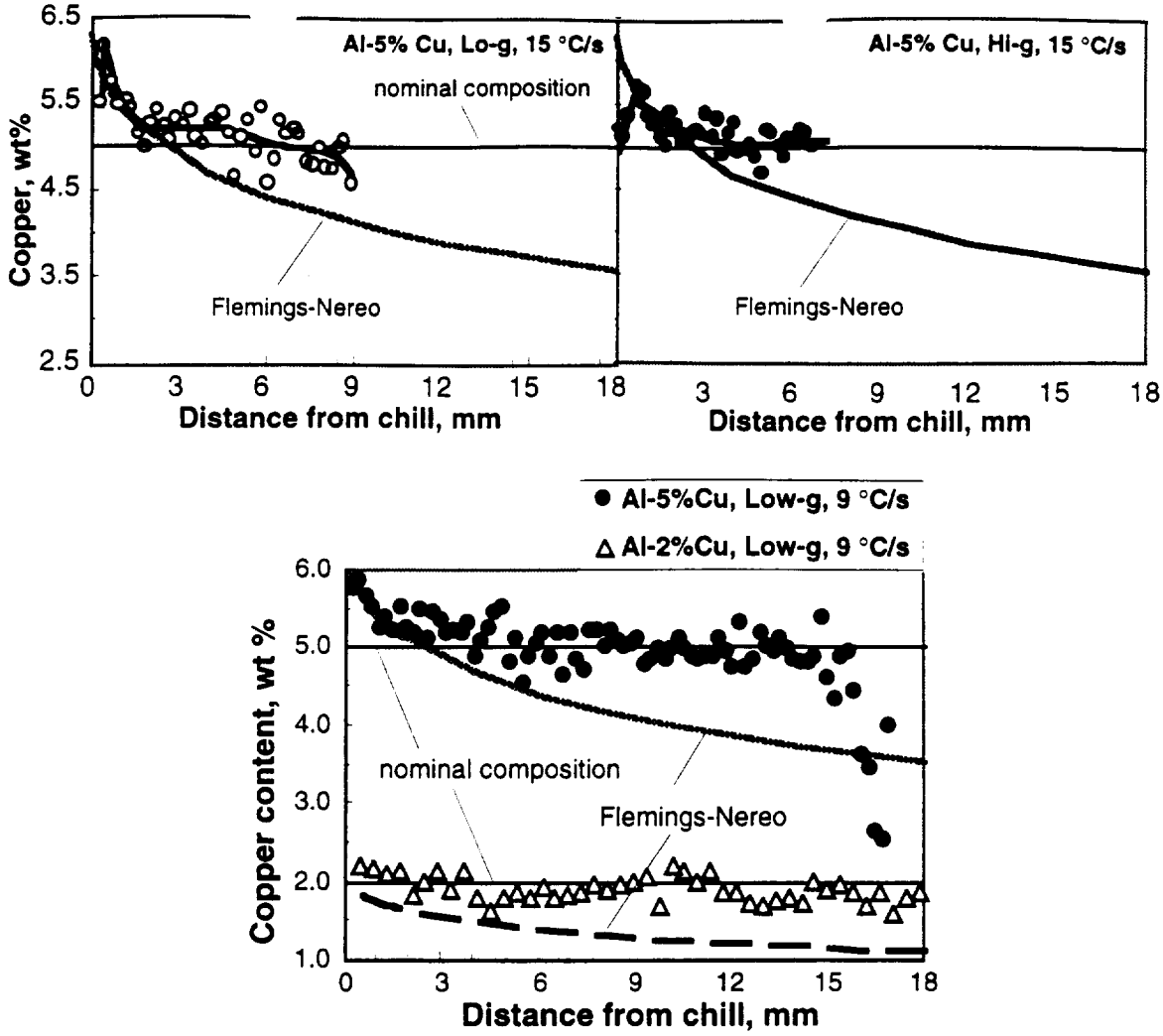

Fig. 8 Evaluation of the Flemings-Nereo model.

Cooling rate has a significant influence on macrosegregation. According to the experimental data, when solidifying under High-g, a lower cooling rate produces more segregation than a high cooling rate. To explain this behavior one must consider the differences both in the microstructure and liquid convection of samples solidified at various cooling rates. Indeed, the presence of some equiaxed grains in the structure, combined with strong natural convection occurring during High-g high-cooling-rate solidification, allows a better redistribution of copper than for the case of the columnar structure resulting during low cooling rate solidification. The process is reversed in Low-g because of the absence of natural convection. Shrinkage flow can move equiaxed grains in the direction of the flow, which is parallel to the longitudinal direction of the sample, resulting in massive segregation. This may explain the apparent higher segregation seen in 2% Cu, 15 °C/s sample solidified in Low-g as compared to the High-g sample (see Fig. 7). A low cooling rate resulting in a mostly columnar structure is less prone to produce shrinkage driven segregation.

Some typical results preliminary calculation with the numer model are shown in Fig. 9. It is seen that, as for the experimental maps in Fig. 6, Low-g solidification results in higher segregation.

(see following pages)

Fig. 9 Calculated map of copper segregation for Al-5% Cu samples solidified under various gravity levels and cooling rates.

Plots of calculated copper content along the central axial direction are presented in Fig. 10. All the calculated plot show the highest segregation to occur at about 5 to 6 mm from the chill. This does not agree well with the experimental data. However, the graphs also show that higher segregation is to be expected in High-g than in Low-g, which is correct. note that the apparent lack of mass balance is simply the result of the one dimension plot. Indeed, the macrosegregation maps in Fig. 9 seem to exhibit good mass balance.

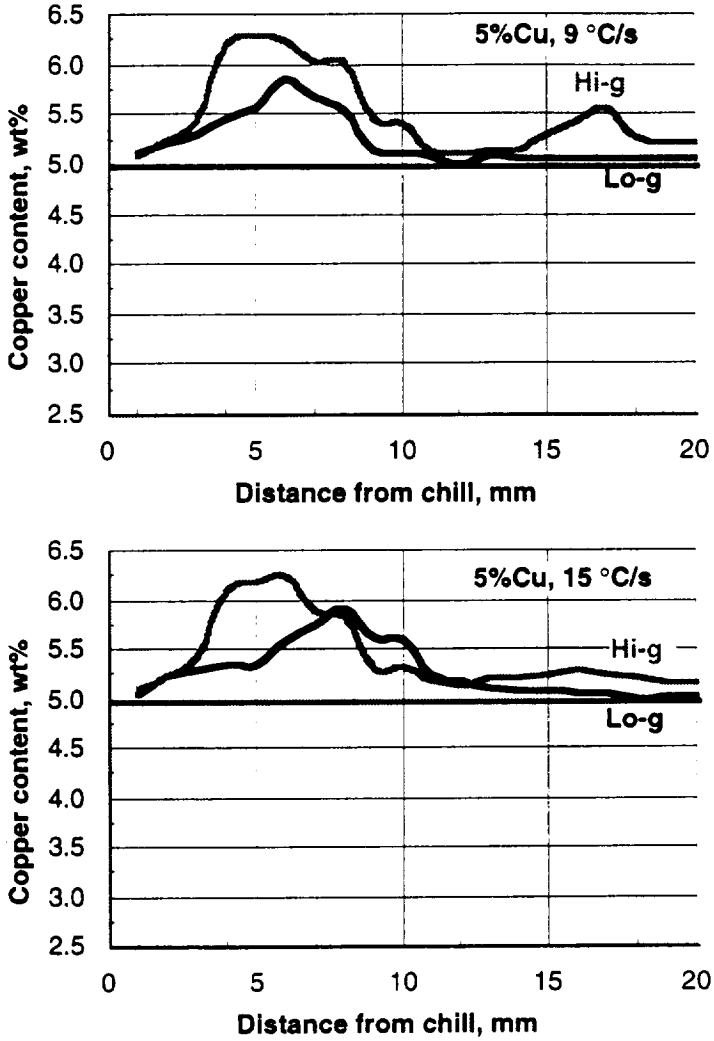

Fig. 10 Calculated axial copper segregation for Al-5% Cu samples solidified under various gravity levels and cooling rates.

From the calculated results it is apparent that the model is steel in need for fine tuning. This effort continues at the University of Alabama, under some additional NASA funding.

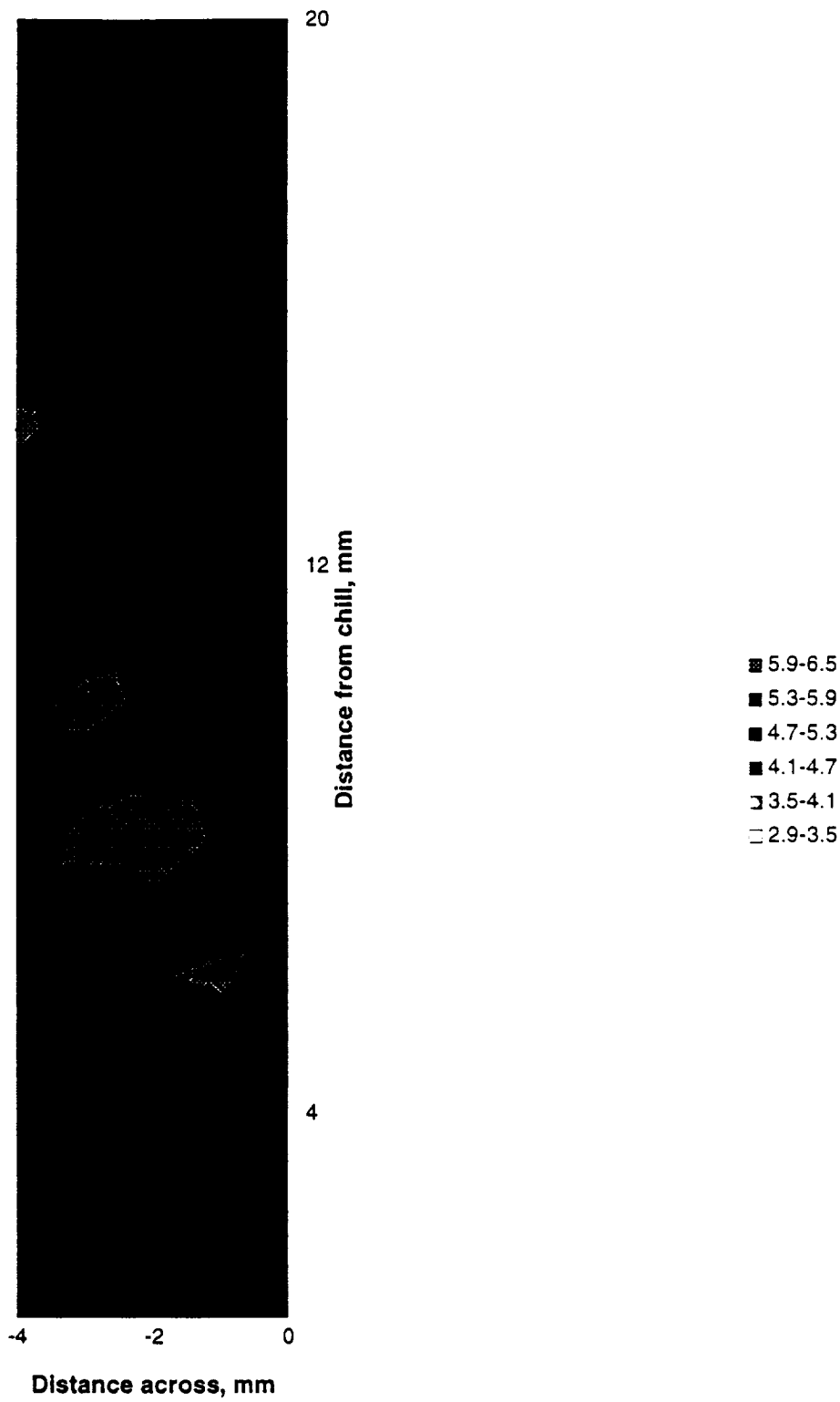

Fig. 9 Macrosegregation map - calculated

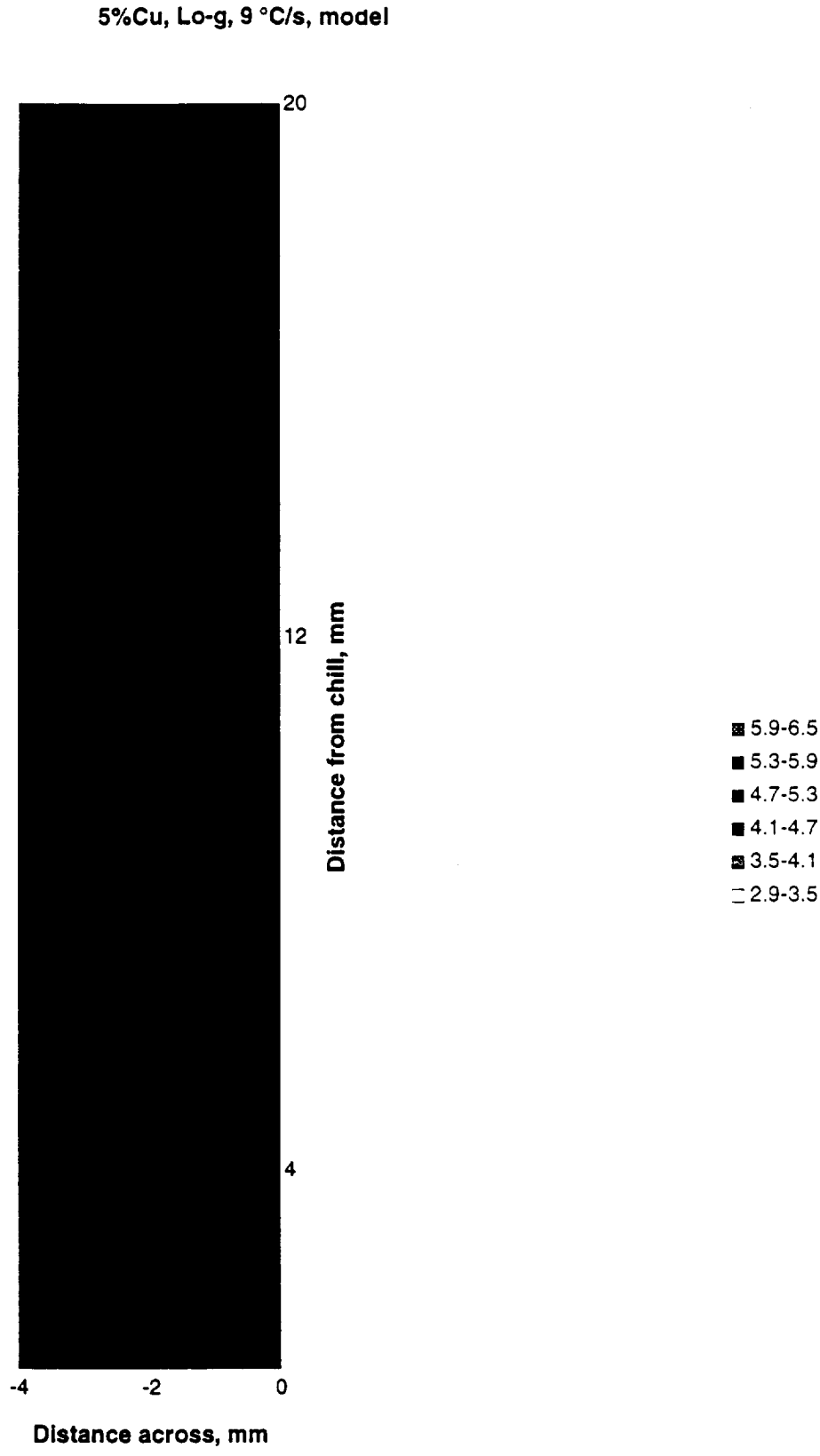

Fig. 8 Macrosegregation map - calculated

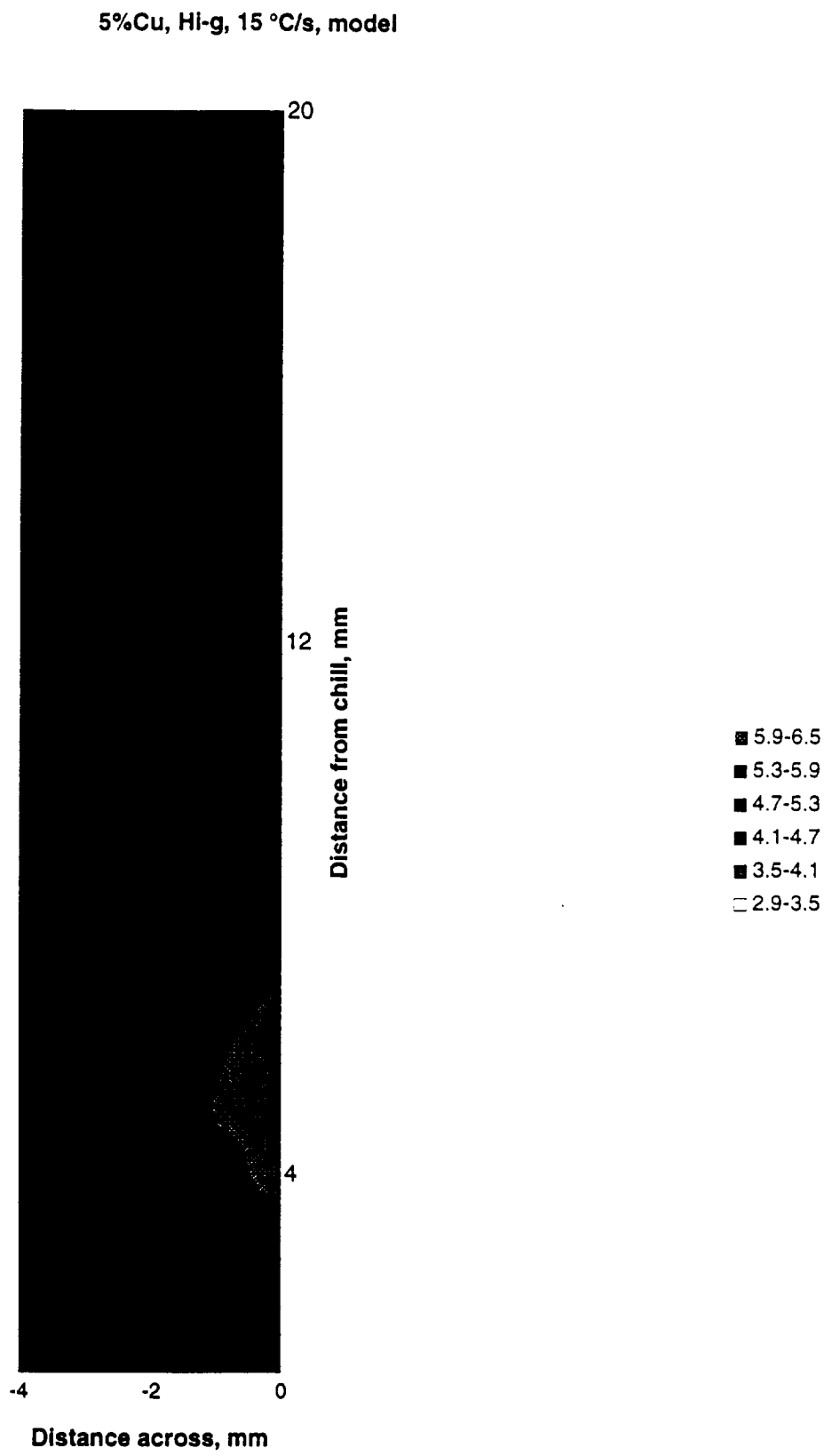

Fig. 9 Macrosegregation map - calculated

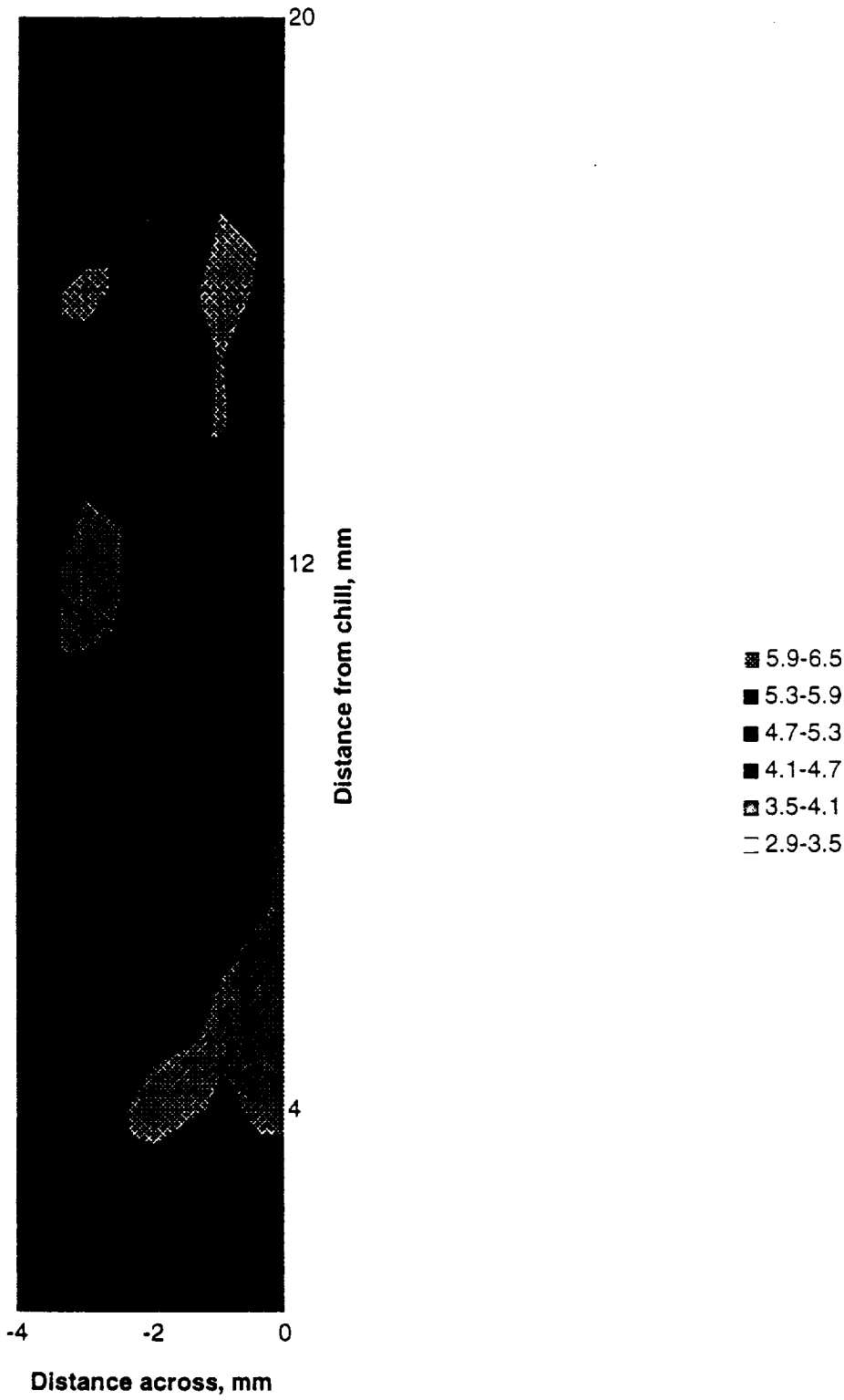

Fig. 9 Macrosegregation map - calculated

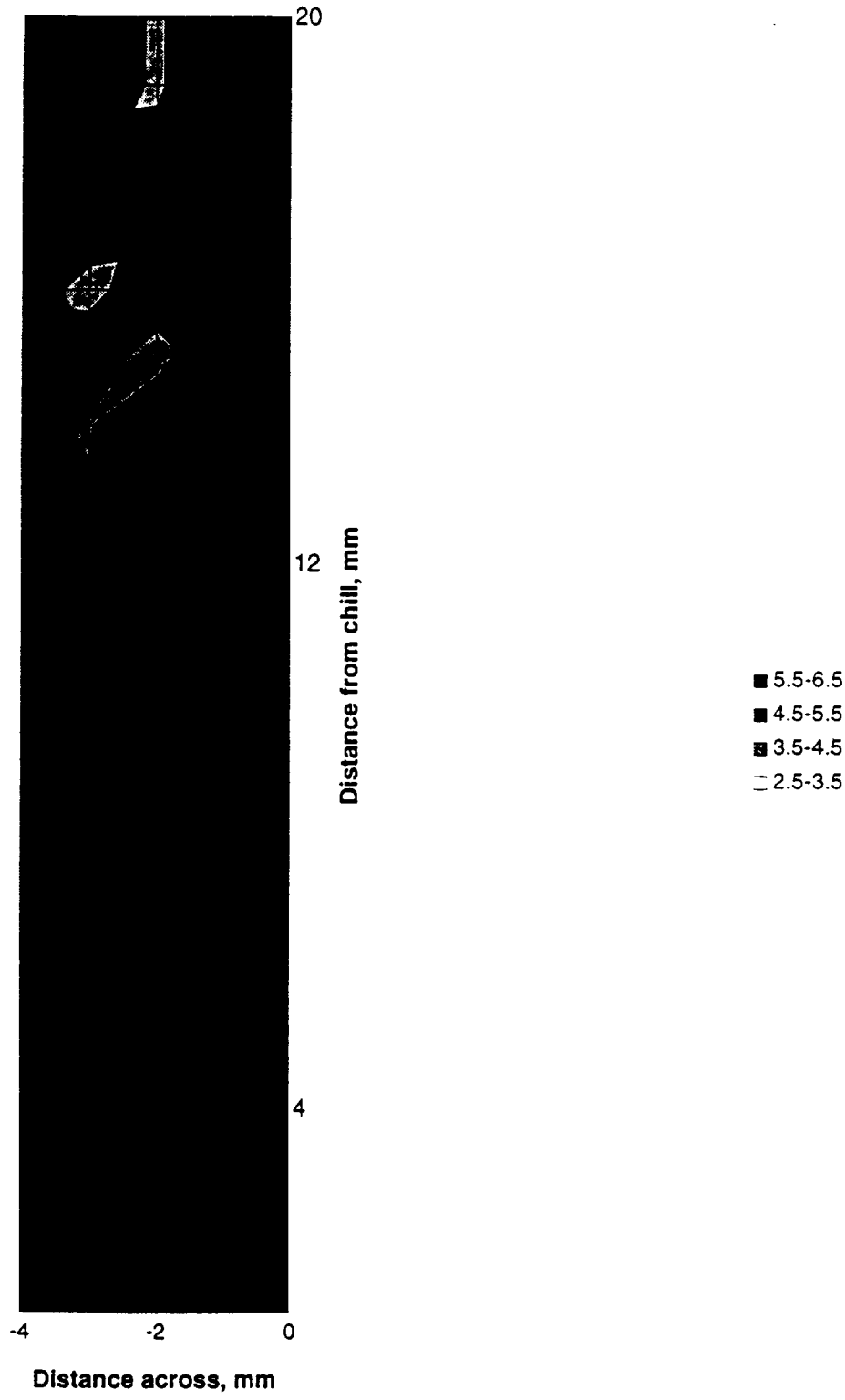

Fig. 8 Macrosegregation map - calculated

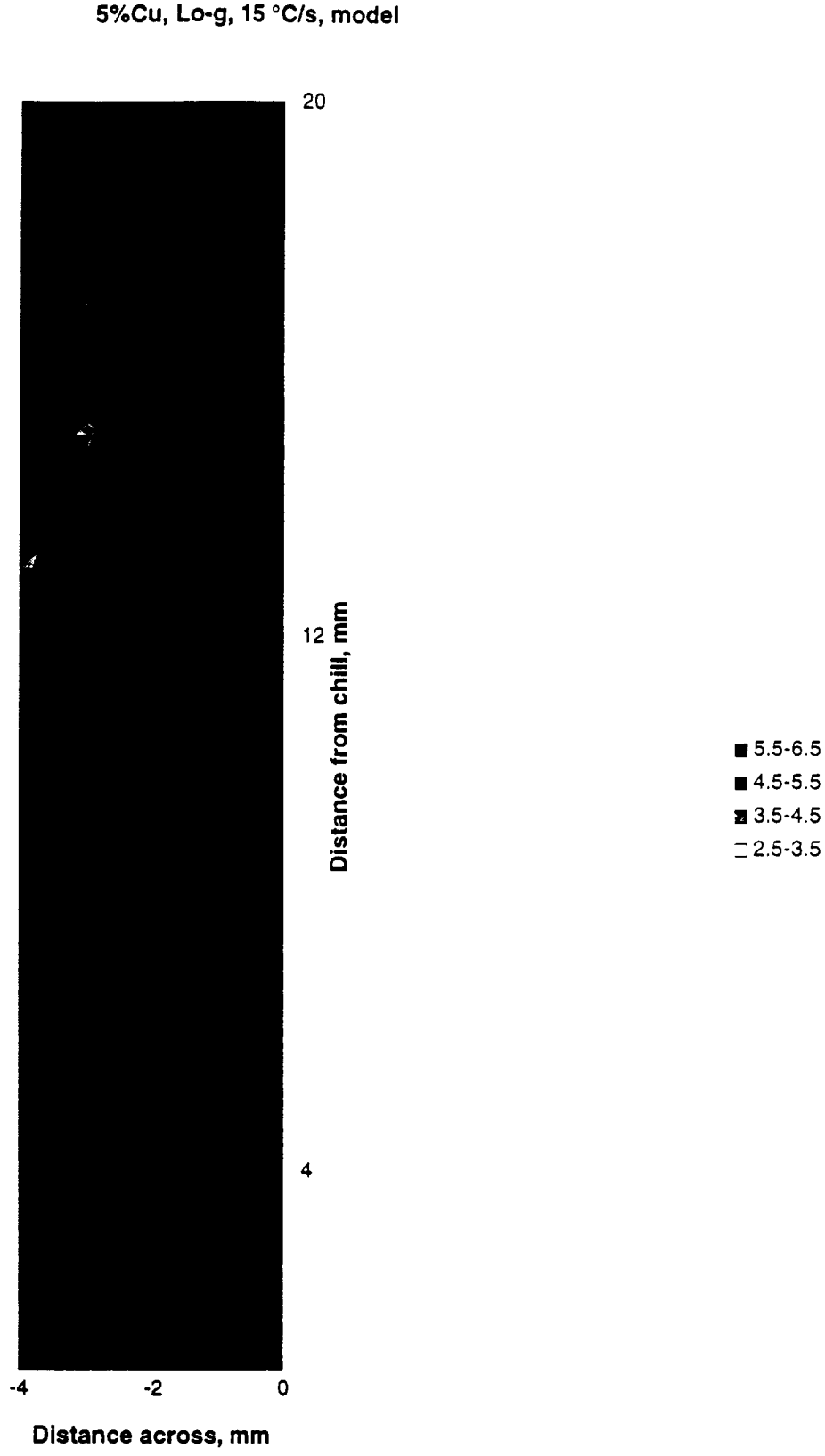

Fig. 8 Macrosegregation map - calculated

6. CONCLUSIONS

Macrosegregation was studied on 10 mm dia. by 20 mm height samples cast from Al-2% Cu and Al-5% Cu alloys, and solidified under terrestrial and low gravity conditions (parabolic flights). It was found, as expected that the gravity level significantly affects macrosegregation. In most cases low-gravity solidification resulted in lower segregation. This is attributed to the absence of natural convection.

The Flemings-Nereo model can predict macrosegregation in the initial stages of Low-g solidification, but increasingly diverges from the experimental data along the sample. Better results are obtained with numerical models that can include the effect of natural convection and of transport of solid particles.

To explain the observed differences in segregation as a function of gravity level and cooling rate, one must consider the microstructure (equiaxed or columnar), the natural convection and the shrinkage induced flow. It is not surprising that, under terrestrial gravity, where fluid flow is driven by solidification shrinkage and natural convection, the macrosegregation pattern is complex and cannot be explained with analytical models.

During this research a large amount of experimental data was collected. At the time this report was written, some characterization as well as some modeling efforts are still in progress.

References

[1] M.C. Flemings and G.E. Nereo, Trans. TMS-AIME, Vol. 239, (1967) pp. 1449-61

[2] M.C. Flemings, R. Mehrabian, and G.E. Nereo, Trans. TMS-AIME, Vol. 242, (1968) pp. 41-49

[3] M.C. Flemings and G.E. Nereo, Trans. TMS-AIME, Vol. 242, (1968) pp. 50-55

[4] H. Kato and J. R. Cahoon, Metall. Trans. A, Vol. 16A, (1985) pp. 579-587

[5] Q.Z. Diao and H. L. Tsai, Metall. Trans. A, Vol. 24A, (1993) pp. 963-973

[6] W.D. Bennon and F. P. Incropera, Int. J. Heat Mass Transfer., Vol. 30, (1987) pp. 2161-70, pp. 2171-87

[7] S. Chang and D.M. Stefanescu, Acta mater., Vol. 44, No.6 (1996) pp. 2227-35

[8] J.J. Favier, J. Berthier, Ph. Arragon, Y. Malmejac, V. T. Khryapov, and I. V. Barmin, Acta Astronautica, Vol. 9, No. 4, (1982) pp. 255-259

[9] A.L. Maples and D.R. Poirier, Metall. Trans. B, Vol. 215 B, (1984) pp. 163-172

[10] M. Krane and F.P. Incropera, Metall. and Materials Trans. A, Vol. 26A, (1995) pp. 2329-2339

[11] L. Nastac and D.M. Stefanescu, Met. Trans. A, Vol. 24A (1993) pp 2107-18

[12] L. Nastac, D.M. Stefanescu and L. Chuzhoy, in *Modelling of Casting, Welding and Advanced Solidification Processes VII*, M. Cross and J. Campbell eds., TMS, (1995) pp. 533-540

[13] S.V. Patankar, *Numerical Heat Transfer and Fluid Flow*, Hemisphere Publishing Corp., New York, (1980)

An Analytical Model for Microsegregation in Open and Expanding Domains

Laurentiu Nastac
Automated Analysis Corp.

Doru Michael Stefanescu
The University of Alabama, Tuscaloosa

Leo Chuzhoy
Caterpillar Inc.

Abstract

A review of existing models for microsegregation shows that there are no analytical models that consider limited diffusion in both liquid and solid phases for an expanding domain (system). Earlier, an analytical mathematical model for microsegregation was introduced for the closed system case. Mass transport by diffusion only was considered, but diffusion in both liquid and solid was assumed. The model proposed in this paper relaxes the assumptions of a closed system. Thus, the contribution of mass transport by fluid flow, and the effects of coarsening and coalescence can be included in microsegregation calculations. The model does not require a prescribed movement of the interface, and therefore, it can be used in microscopic modeling of solidification. The derivation assumed spherical geometry of the domain. Thus, it is possible to calculate microsegregation at the level of equiaxed dendrites. The importance of an open and expanding domain assumptions was studied by comparing results obtained with the present model with calculation based on the closed system assumptions. The microsegregation model was coupled with a macro transport -- transformation kinetics code to compare the calculated results with experimental results for spheroidal graphite iron castings.

Acknowledgments: This work was supported by a grant from NASA, contract no. NCC8-57 and a grant from Caterpillar Inc., contract no. RBJ 23366.

Modelling of Casting, Welding and Advanced Solidification Processes VII
Edited by M. Cross and J. Campbell
The Minerals, Metals & Materials Society, 1995

Introduction

All existing analytical microsegregation models are based on the "closed system" assumption, *i.e.* no net mass enters or leaves the domain during solidification. Such assumption may lead to erroneous calculations in many cases. Few models tackle coarsening and coalescence phenomena that occur during solidification. The purpose of this paper is to establish the impact of the "open system" assumption (mass transport in and out of the element) and of the "expanding system" assumption (coarsening and coalescence) on microsegregation.

Model Development

Assumptions, governing equations and boundary conditions

Consider a macro-volume element within the solidifying metal. It can be for example of the mesh size of a macro-heat transfer model for solidification of castings. Within this macro-element the temperature is assumed uniform and is obtained from the solution of the thermal field. The macro-element is further subdivided in a number of spherical micro-elements (Fig. 1 a). Within each of these elements of radius R_f, a spherical equiaxed grain of radius R_γ^t is growing until the whole volume is filled. If the particular case of SG iron is considered, a graphite spheroid of radius R_G is growing within the spherical austenite grain of radius R_γ^t.

The γ-G aggregate solidifies by simultaneous growth of the graphite and austenite phases. The assumed geometry and the schematic solute concentration profiles developed in the solid and liquid phases for an element are presented in Fig. 1 b. Micro-diffusion transport within the element starts concomitantly with solidification. Coarsening and/or coalescence are allowed to take place during solidification.

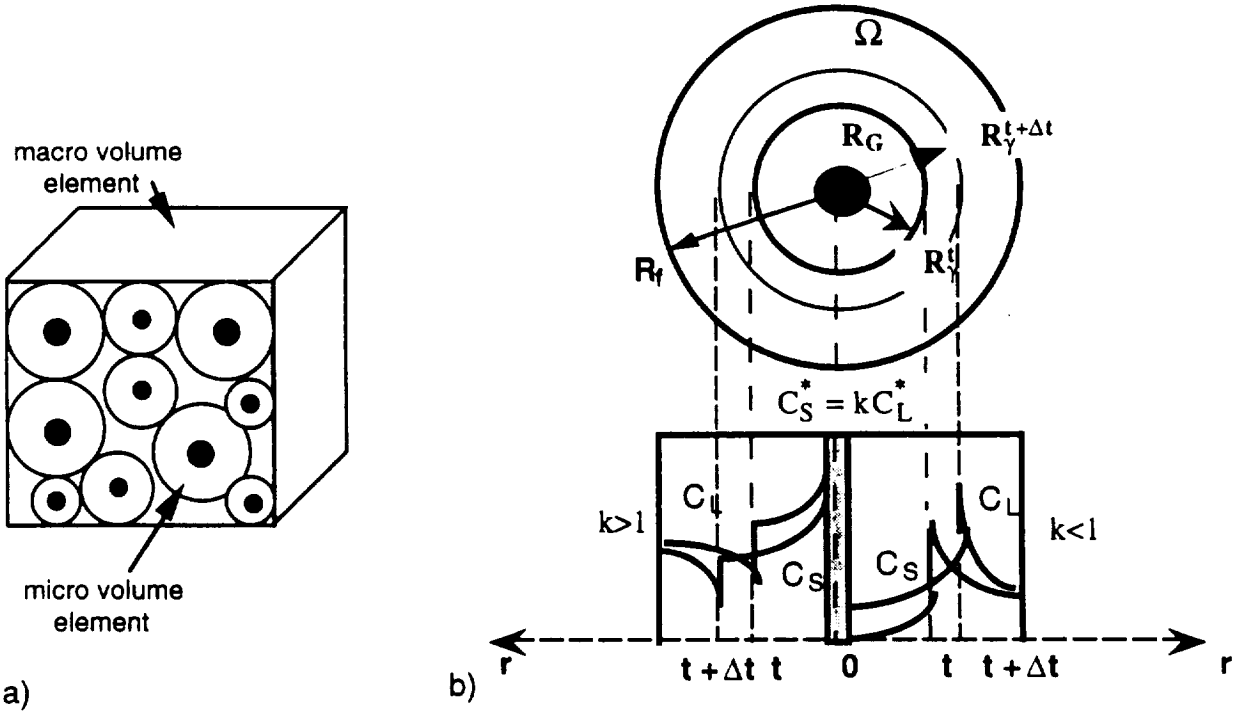

Fig. 1. Schematic representation of (a) a solidifying macro volume and (b) of a micro volume element as well as of the associated concentration profile corresponding to a partition ratio greater or lower than one.

The problem to solve is to calculate the composition profiles in both the solid and the liquid during solidification. Then, the microsegregation ratio can be calculated. At the nucleation temperature, $T_n \leq T_L$, the first solid formed has a solute concentration $k\,C_o$, where k is the partition ratio. The liquid in the vicinity of the solid/liquid interface is either enriched in (if $k < 1$), or depleted of (if $k > 1$) solute. The final liquid fraction will have a solute concentration that depends on the diffusion coefficients in the solid and liquid phases, growth velocity of the grain, coarsening and coalescence, as well as macro-convective flow through macrosegregation. The main assumptions of the model are as follows:

(1) Solute transport in both phases is by diffusion with diffusion coefficients independent on concentration. Therefore, the double boundary problem must be solved for C_S (r, t) and C_L (r, t). The solute concentrations in the solid (S) and liquid (L) phases must satisfy Fick's second law:

$$\frac{\partial C_S}{\partial t} = \frac{1}{r^m}\frac{\partial}{\partial r}\left(r^m D_S \frac{\partial C_S}{\partial r}\right) \qquad \text{and} \qquad \frac{\partial C_L}{\partial t} = \frac{1}{r^m}\frac{\partial}{\partial r}\left(r^m D_L \frac{\partial C_L}{\partial r}\right) \tag{1}$$

where, D_S and D_L are the diffusion coefficients in the solid and liquid phases, respectively, and m is an exponent (m=2 for spherical geometry, m=1 for cylindrical geometry, and m=0 for plate geometry).

(2) The material is incompressible and the densities in both phases are constant.

(3) The solid-liquid interface is planar and under local equilibrium:

$$C_S^* = k C_L^* \tag{2}$$

where, the superscript * denotes values at the interface. From Eq (2) two boundary conditions, unknown *a priori.*, are obtained:

$$C_S[R^*(t), t] = C_S^* \qquad \text{and} \qquad C_L[R^*(t), t] = C_L^* \tag{3}$$

(4) There is solute flow into or out of the volume element considered ("open system"). Thus microsegregation calculation can include the contribution of mass transport by convective flow, and the effects of coarsening and coalescence. The overall mass balance for an open system can be written in integral form as:

$$\frac{1}{\rho V_\Omega}\int_{V_\Omega} \rho\, C(r, t)\, dV_\Omega = \langle C \rangle \tag{4}$$

where $\langle C \rangle$ is the local mass average concentration over the volume element, and V_Ω is the volume of the element over which the mass balance is computed. Note that the volume of the element is varying in time. Coarsening and coalescence will impose an increase of this volume ("expanding system"). Assuming, for the sake of notation simplification, that the densities of the solid and liquid phases are not only constant, but also equal:

$$v_{\Omega(t)}\langle C \rangle = \int_0^{R^*(t)} 4\pi r^2 C_S(r, t)\, dr + \int_{R^*(t)}^{R_f(t)} 4\pi r^2 C_L(r, t)\, dr \tag{5}$$

Eq (5) is used to couple the concentration fields in both the solid and liquid phases.
The boundary conditions for the finite open system are written as:

$$D_S \frac{\partial C_S}{\partial r} = 0\ ,\ \text{at } r = 0 \qquad \text{and} \qquad D_L \frac{\partial C_L}{\partial r} = V_c[\langle C(t) \rangle - C_L(R_f)] + \frac{R_f}{m+1}\frac{\partial \langle C \rangle}{\partial t}\ ,\ \text{at } r = R_f \tag{6}$$

where V_c is coarsening velocity. In the boundary condition for the liquid phase, the first term on the right hand side represents the influence of coarsening and the second term is the contribution of convective fluid flow on microsegregation. Due to the rapid liquid diffusion it is computationally convenient to include it in the flux boundary condition at $r = R_f$ rather than in the flux balance [1]. The flux boundary condition describes by Eq. (6) is obtained by differentiating in time Eq. (5) and applying the Leibnitz's integral formula for differentiation. In non dimensional form, the flux boundary condition at $r = R_f$ is:

$$\frac{\partial C_L}{\partial a} = Pe_c[\langle C(t) \rangle - C_L(R_f)] + f(t) \quad \text{with} \qquad a = \frac{r}{R_f}$$

$$f(t) = \frac{R_f^2}{(m+1) D_L}\frac{\partial \langle C \rangle}{\partial t} \qquad Pe_c = \frac{V_c R_f}{D_L} \tag{7}$$

(5) The initial concentration in the liquid, C_o, is constant for each volume element (micro - scale), but it is variable at the macro - scale level (casting).

Finally, the solution of the coupled double boundary value problem can be obtained by solving Eqs. (1) with the boundary conditions described by Eqs. (3), (5) and (7). The liquid and solid solutal fields are coupled through Eq (5). The following initial conditions are used:

$$C_S(r,t_o) = k C_o(x,y,z,t_o) \qquad \text{and} \qquad C_L(r, t_o) = C_o(x, y, z, t_o) \tag{8}$$

where t_o is the time when the local solidification starts.

Solution

The solution of 'Fickian' diffusion for a spherical element during solidification, consists of the following equations:

$$C_S(r,t) = k C_L^*(t) + k\left[C_o - C_L^*(t)\right] \sum_{n_S=1}^{\infty} \frac{B'_{n_S}}{r} \sin\left[\sqrt{\lambda'_{n_S}}\, r\right] \exp\left[-\lambda'_{n_S} D_S t\right] \tag{9}$$

$$C_L(r,t) = C_L^*(t) + \left[C_o - C_L^*(t)\right] \sum_{n_L=1}^{\infty} \frac{B'_{n_L}}{r} \sin\left[\sqrt{\lambda'_{n_L}}\left(r - R^*\right)\right] \exp\left[-\lambda'_{n_L} D_L t\right] + A(t) R_f \left(\frac{1}{R^*} - \frac{1}{r}\right) \tag{10}$$

$$\text{with} \quad B'_{n_S} = 2 R^* \frac{(-1)^{n+1}}{n_S \pi} \qquad B'_{n_L} = \frac{2 R^*}{\alpha_n} \qquad A(t) = Pe_c \langle C(t) \rangle + \frac{R_f^2}{3 D_L} \frac{\partial \langle C \rangle}{\partial t} \tag{11}$$

$$\lambda'_{nS} = \left[\frac{n_S \pi}{R^*}\right]^2 \qquad \lambda'_{nL} = \left[\frac{\alpha_n}{R_f - R^*}\right]^2 \qquad \tan \alpha_n = \frac{R_f \alpha_n}{R_f - R^*} \frac{1}{1 - Pe_c} \tag{12}$$

The interface solid concentration, is given by:

$$C_S^* = C_S^*(\text{close}) + C_S^*(\text{open}) \tag{13}$$

$$\text{with} \quad C_S^*(\text{close}) = k C_o \frac{1 - 3\left[k I_S + I_L\right]}{1 - 3\left[k I_S + I_L\right] - f_S(1-k)} \qquad f_S = \left(R^*/R_f\right)^3 \tag{14}$$

$$C_S^*(\text{open}) = k \frac{\langle C(t) \rangle - C_o - \frac{A(t)}{\eta}\left(1 - \frac{3}{2}\eta + \frac{1}{2}\eta^3\right)}{1 - 3\left[k I_S + I_L\right] - f_S(1-k)} \qquad \eta = R^*/R_f \tag{15}$$

$$I_S = \frac{2 f_S}{\pi^2} \sum_{n=1}^{\infty} \frac{1}{n^2} \exp\left[-\left(\frac{n\pi}{f_S^{1/3}}\right)^2 \frac{D_S t}{R_f^2}\right] \qquad I_L = 2 f_S^{2/3}\left(1 - f_S^{1/3}\right) \sum_{n=1}^{\infty} \frac{1}{\alpha_n^2} \exp\left[-\left(\frac{\alpha_n}{1 - f_S^{1/3}}\right)^2 \frac{D_L t}{R_f^2}\right] \tag{16}$$

where α_n is the n-th root of the equation $\alpha_n / \tan(\alpha_n) = \left(1 - f_s^{1/3}\right)(1 - Pe_c)$. The mathematical assumptions involved in derivation of Eqs. (9)-(16) are in line with those described in refs. [2, 3]. They are valid for $Pe_L = V R_f / D_L < \pi^2$. For the case of "closed system" and no coarsening the microsegregation model (Eq. 13) reduces to that derived in ref. [2].

Since no assumption on the evolution of the fraction of solid was used in the present derivation, any transformation kinetics model can be used to calculate the movement of the interface. In this paper the fraction of solid is calculated through the heat transfer--transformation kinetics model for SG iron [4]. The radius of the austenite-liquid interface (austenite shell) is given by:

$$R_\gamma = \int_0^t V_\gamma \, dt = D_C^{(\gamma)} \int_0^t \frac{R_G R_\gamma^{-1}}{R_\gamma - R_G} \frac{C^{(L/\gamma)} - C^{(G/\gamma)}}{C^{(\gamma/L)} - C^{(L/\gamma)}} \, dt \tag{17}$$

where V_γ is the growth velocity of the austenite phase, $D_C^{(\gamma)}$ is the diffusion coefficient of carbon in austenite, $C^{(G/\gamma)}$ is the concentration of carbon in the austenite matrix at the graphite/austenite interface, $C^{(L/\gamma)}$ is the concentration of carbon in the austenite matrix at the

liquid/austenite interface, and $C^{(\gamma/L)}$ is the concentration of carbon in the liquid at the liquid/austenite interface. R_G and R_γ are the radii of the graphite spheroid and of the austenite shell, respectively. They have been obtained in the previous time step of the numerical calculation.

Coupling of micro- and macro- segregation

The general methodology for coupling between micro- and macro- segregation (open system) is described in ref. [5] for equilibrium (lever rule) and non equilibrium (Scheil) cases. For limited diffusion in both solid and liquid phases, the link between micro- and macro-segregation done through use of the following equation:

$$\overline{V}\ \mathrm{grad}\,\langle C_L\rangle^L + \frac{\partial \langle C\rangle}{\partial t} = 0 \qquad \text{where } \langle C\rangle = \langle C_S\rangle^S f_S + \langle C_L\rangle^L f_L \qquad \overline{V} = f_L V_L \tag{18}$$

$$\text{and } \langle C_S\rangle^S = k C_L^* + 6k\left[C_o - C_L^*\right] \sum_{n_S=1}^{\infty} (n_S \pi)^{-2} \exp\left[-\lambda'_{n_S} D_S t\right] \tag{19}$$

$$\langle C_L\rangle^L = C_L^* + \frac{6\left[C_o - C_L^*\right]R^{*2}}{R_f^2 + R^* R_f + R^{*2}} \sum_{n_L=1}^{\infty} \alpha_n^{-2} \exp\left[-\lambda'_{n_L} D_L t\right] + A(t)\left(\frac{R_f}{R^*} - \frac{3}{2}\frac{R_f\left(R^* + R_f\right)}{R_f^2 + R^* R_f + R^{*2}}\right) \tag{20}$$

where $\overline{V}$ is the average macroscopic velocity over the volume element, and V_L is the superficial velocity. Their origin is the shrinkage flow, the buoyancy flow (thermosolutal convection), and the relative motion flow of the liquid/solid interface. Eq. (18) assumes no diffusion at the macro-scale level. It is similar with that derived by Beckermann and Viskanta [6]. Note also that Eq. (18) represents an implicit link between micro- and macro- segregation. The concentration gradient in the liquid phase that contributes to the convective term (first term in Eq. 18) is obtained from the macrosegregation model. The second term in Eq.(18) is used to solve microsegregation (see Eq. 11) and is obtained through both the micro- and macro- segregation models. The governing equations for macroscopic transport include the conservation equations for mass, momentum, energies, and species for the geometry of interest. They are solved by the control volume method.

Model Evaluation

To evaluate the contribution of the "open system" and of coarsening on microsegregation a theoretical sensitivity analysis was performed. The variation of the interface liquid concentration and the fraction of eutectic was calculated for a hypothetical system using different process variables and assumptions with the model. The main data and variables used in calculation, and the calculated fraction of eutectics, are summarized in Table 1. Constant growth and coarsening velocities for each case were assumed so that, both the solidification time, t_f and th final grain radius, R_f, were the same. A linear variation with time for the local average concentration was assumed to allow for the solute to either enter or leave the domain. For instance, "Open+10%C+10%R" means that the local average concentration is linearly increased (solute enters the domain) from 100% (initial value at the onset of solidification) to maximum 110% (end of solidification), and 10% linear increase in the grain radius (coarsening) is allowed.

The Scheil model (closed system, complete diffusion in liquid, no diffusion in solid) was used as a basis for comparison. It is apparent from Table 1 and Fig. 2 that the results obtained with the Scheil model and the present model applied to the closed system are very close. Small discrepancies were observed at the end of solidification when the Scheil model predicted larger amount of eutectic than the proposed model.

However, large differences in the prediction of both interface liquid concentration and fraction of eutectic were observed, when the "open system" assumption were used (Table 1 and Fig. 3). This clearly emphasizes the importance of relaxing the "open system" assumption. When only coarsening and/or coalescence were introduced, small fluctuations in the results were observed. This is because, both the size of the final domain and solidification time were maintained constant, such that the overall micro-diffusion was not much affected. Note that considering

Table 1. Sensitivity analysis of the microsegregation model. Main data used for calculation are: C_o=1.0, C_{eut}=10.0, k=0.1, $D_L=10^{-9}$, $D_S=10^{-12}$.

Model	t_f=100 s, R_f=100 mm				t_f=10 s, R_f=50 mm			
	f_{eut}	Vg, μm/s	Vc, μm/s	R_{fo}, μm	f_{eut}	Vg, μm/s	Vc, μm/s	R_{fo}, μm
Scheil	0.0774	-	-	-	0.0774	-	-	-
Close	0.0588	1	0	100	0.0703	5	0	50
Open+10%C*+0%R**	0.0703	1	0	100	0.0817	5	0	50
Open+10%C+10%R	0.0728	0.9	0.1	90	0.7098	4.5	0.5	45
Open+10%C+100%R	0.0720	0.5	0.5	50	0.0810	2.5	2.5	25
Open+50%C+0%R	0.1097	1	0	100	0.1208	5	0	50
Open+50%C+10%R	0.1056	0.9	0.1	90	0.1093	4.5	0.5	45
Open+50%C+100%R	0.1109	0.5	0.5	50	0.1199	2.5	2.5	25
Open-10%C+0%R	0.0530	1	0	100	0.0588	5	0	100
Open-10%C+0%R	0.0516	0.9	0.1	90	0.0589	4.5	0.5	45
Open-10%C+00%R	0.0540	0.5	0.5	50	0.0630	2.5	2.5	25
Open-50%C+0%R	0.0119	1	0	100	0.0179	5	0	100
Open-50%C+10%R	0.0181	0.9	0.1	90	0.0100	4.5	0.5	45
Open-50%C+100%R	0.0120	0.5	0.5	50	0.0210	2.5	2.5	25
Open 0%C+10%R	0.0623	0.9	0.1	90	0.0694	4.5	0.5	45
Open 0%C+100%R	0.0730	0.5	0.5	50	0.0720	2.5	2.5	25

* C is the solute (X% of local average concentration) that can either enter (+) or leaves (-) the system
** R is grain coarsening (+X% of final grain radius, R_f); R_{fo} is the initial grain radius.

only coarsening and/or coalescence without allowing the solute to enter in the domain may be misleading. Both coarsening and "open system" have to be considered (the summation of both terms in Eq. 11). Then, the effect of coarsening and/or coalescence on microsegregation can be correctly analyzed. As shown in Table 1, there are significant differences in the prediction of the fraction of eutectic between expandable and non expandable domains.

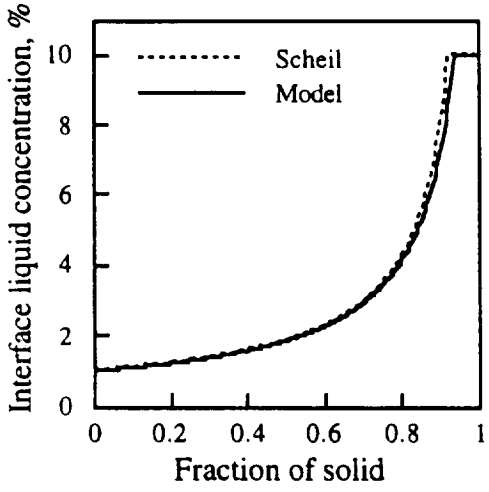

Fig. 2. Variation of interface liquid concentration calculated with Scheil and proposed model (closed system case).

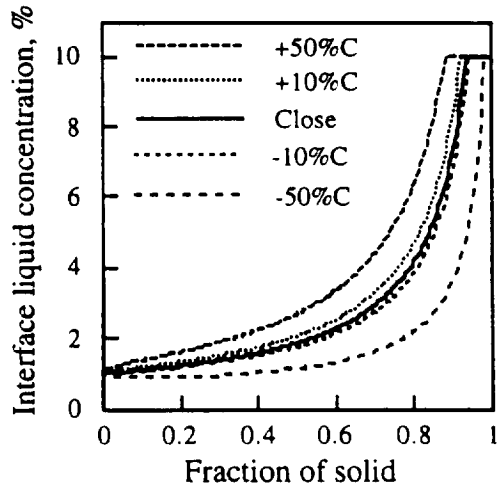

Fig. 3. Variation of interface liquid concentration calculated with proposed model (closed and open system).

Model Validation

Validation of the model was performed using the experimental data of Boeri and Weinberg [7]. The diameter of the measured samples was 15 mm. The physical constants used for calculation are those given in Table 2.

The characteristic distance between equiaxed dendrite center and the last liquid to solidify, that is the final radius in this model (R_f), is 75 mm, and the local solidification time (t_f) is 30 s [7]. Since the eutectic temperature range is small, the diffusion coefficients were considered to be independent on temperature. The diffusivity values at the equilibrium eutectic temperature (T_E = 1155 °C) were used.

Table 2. Data used in calculation of concentration profiles in SG iron

Element	D_S, m^2s^{-1}	D_L, m^2s^{-1}	k	Refs.
Cu	$5x10^{-12}$	$3x10^{-9}$	1.4	[7, 8]
Mn	$6x10^{-13}$	$4.5x10^{-9}$	0.70	[7, 8]

The redistribution of Mn and Cu in SG iron within a spherical element containing one graphite spheroid was calculated with the proposed model for the open and closed system cases. The results are compared with the experimental data [7] in Figs. 4 and 5. Manganese produces normal microsegregation (k<1), while copper produces inverse microsegregation (k >1) during solidification of SG iron. For copper the model predicts lower concentration than the experimental values. A possible explanation is that the partition coefficient may vary during solidification [8]. It may be dependent on composition and convection in the liquid phase. Thus, for accurate prediction of microsegregation it is necessary to have correct data for k. As shown in ref. [8], much better agreement was obtained for copper redistribution when a variable k was introduced. Unfortunately, the equation for the variation of k [8] was strictly developed for the closed system assumption and could not be used in this analysis. As can also be seen from Figs. 4 and 5, similar results are observed for redistribution of Cu and Mn for both open and close system assumptions. This is because the convective flow, and therefore macrosegregation developed during solidification of SG iron thin castings (15 mm ID), were small, while the heat extraction rate was high.

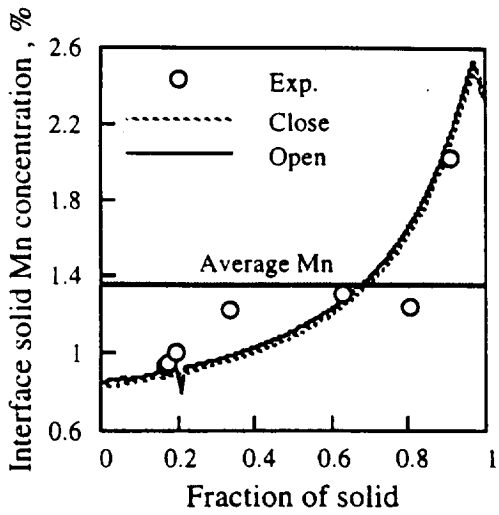

Fig. 4. Comparison of calculated (present model) and experimental [7] interface solid Mn concentration in SG iron.

Local average concentration profiles of Cu and Mn in the center of the samples are plotted in Fig. 6. Small variations (< 1%) in the local average concentrations during solidification can be observed. An interesting feature can be observed in the concentration profiles of Cu and Mn for the open system assumption. At f_S=0.2, the interface and local average concentrations of Cu increases abruptly, while those of Mn show a sudden decrease.

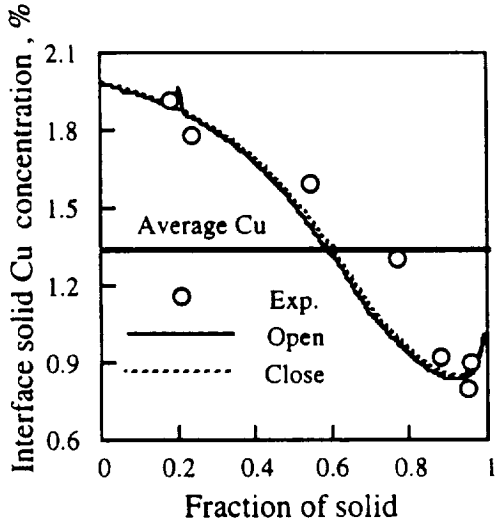

Fig. 5. Comparison of calculated (present model) and experimental [7] interface solid Cu concentration in SG iron.

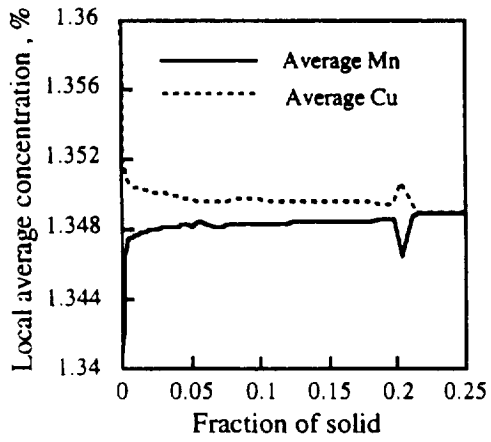

Fig. 6. Variation of local average concentrations of Mn and Cu calculated with present model during solidification of SG cast iron. Initial concentrations of Mn and Cu are 1.34 and 1.36, respectively.

This apparently strange behavior can be explained through Fig. 7, where convective and isotherm velocity, as well as the ratio between the two are represented. Here, the combined influence of convective and heat flow through the evolution of the fraction of solid affects macrosegregation (local average concentration) and therefore, microsegregation. Note the sensitivity of the

microsegregation m\ .l in following up the local variation of . .crosegregation.

Concluding Remarks

A comprehensive analytical micro-segregation model, that considers diffusion in both solid and liquid phases, and relaxes the closed system assumption, was introduced. It solves the 'Fickian' diffusion with time-independent diffusion coefficients and non zero-flux boundary conditions for systems solidifying with equiaxed morphology. The model that has general validity takes into account solute transport in the solid and liquid phases and includes overall solute balance. Since the model does not require a prescribed movement of the interface, it can be used for microscopic modeling of solidification. The model allows calculation of liquid and solid compositions, during and after solidification, for spherical geometry (equiaxed grains). It also includes coarsening and coalescence that take place during solidification. It can be used for concentration profile calculations for systems that solidify with equiaxed grains, whether eutectic (*e.g.*, lamellar graphite-austenite, Al-Si) or dendritic (*e.g.*, Al-alloys, Fe-low C alloys, superalloys).

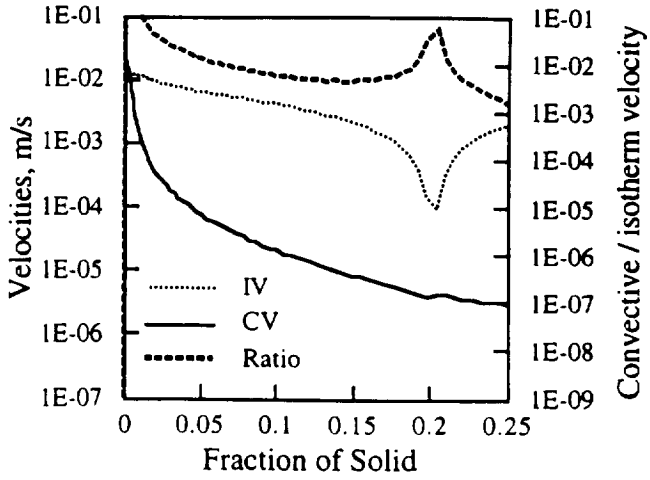

Fig. 7. Variation of superficial convective velocity (CV), isotherm velocity (IV), and ratio between CV and IV during solidification of SG iron. Isotherm velocity is calculated as the ratio between the local cooling rate and local thermal gradient in the center of the casting.

Nomenclature

- C solute concentration [wt.%]
- C_o initial solute concentration [wt.%]
- D diffusion coefficient [$m^2 s^{-1}$]
- R_n nucleus radius [m]
- R radius [m]
- V_Ω volume of element [m^3]
- V_g growth velocity [$m s^{-1}$]
- V_c coarsening velocity [$m s^{-1}$]
- a dimensionless radius
- f_S fraction of solid
- k equilibrium partition ratio
- r radius coordinate [m]
- t time [s]
- t_f local solidification time [s]
- η dimensionless interface position

General Subscripts/Superscripts

S: solid L: liquid f: final *: at interface

References

1. S. Sundarraj and V. R. Voller, HTD-Vol. 218/AMD-Vol. 139, *ASME Conference*, (1992), 35- 42.
2. L. Nastac and D. M. Stefanescu, *Met. Trans. A*, Vol. 24A, (1993), 2107- 18.
3. L. Nastac, S. Chang, D. M. Stefanescu, and L. Hadji, in *Microstructural Design by Solidification Processing*, ed. E. J. Lavernia and M. N. Gungor, The Minerals, Metals & Materials Society, (1992), 57- 75.
4. S. Chang, D. Shangguan, and D. M. Stefanescu, *Met. Trans. A.*, vol. 23A, (1992), 1333- 46.
5. M. Rappaz and V. Voller, *Met. Trans.*, Vol. 21A, (1990), 749- 53.
6. C. Beckermann and R. Viskanta, *Phys. Chem. Hydrodyn.*, vol. 10, (1988), 195- 213.
7. R. Boeri and F. Weinberg, *AFS Transactions*, vol. 89, (1989), 179- 84.
8. L. Nastac and D. M. Stefanescu, *AFS Transactions*, Vol. 134, (1993), 933- 38.